Department of Precision and Microsystems Engineering

Experimental Characterization of the Young's Modulus of MCF-7 Cancer Cells in Cell-Cell and Cell-Substrate Configurations using AFM

Monique Nguyen

Report no	: 2024.103
Coach	: dr. ir.V.U.Shastri
Professor	: dr.M.K.Ghatkesar
Specialisation	: Mechatronic System Design
Type of report	: Masters Thesis
Date	: December 2, 2024

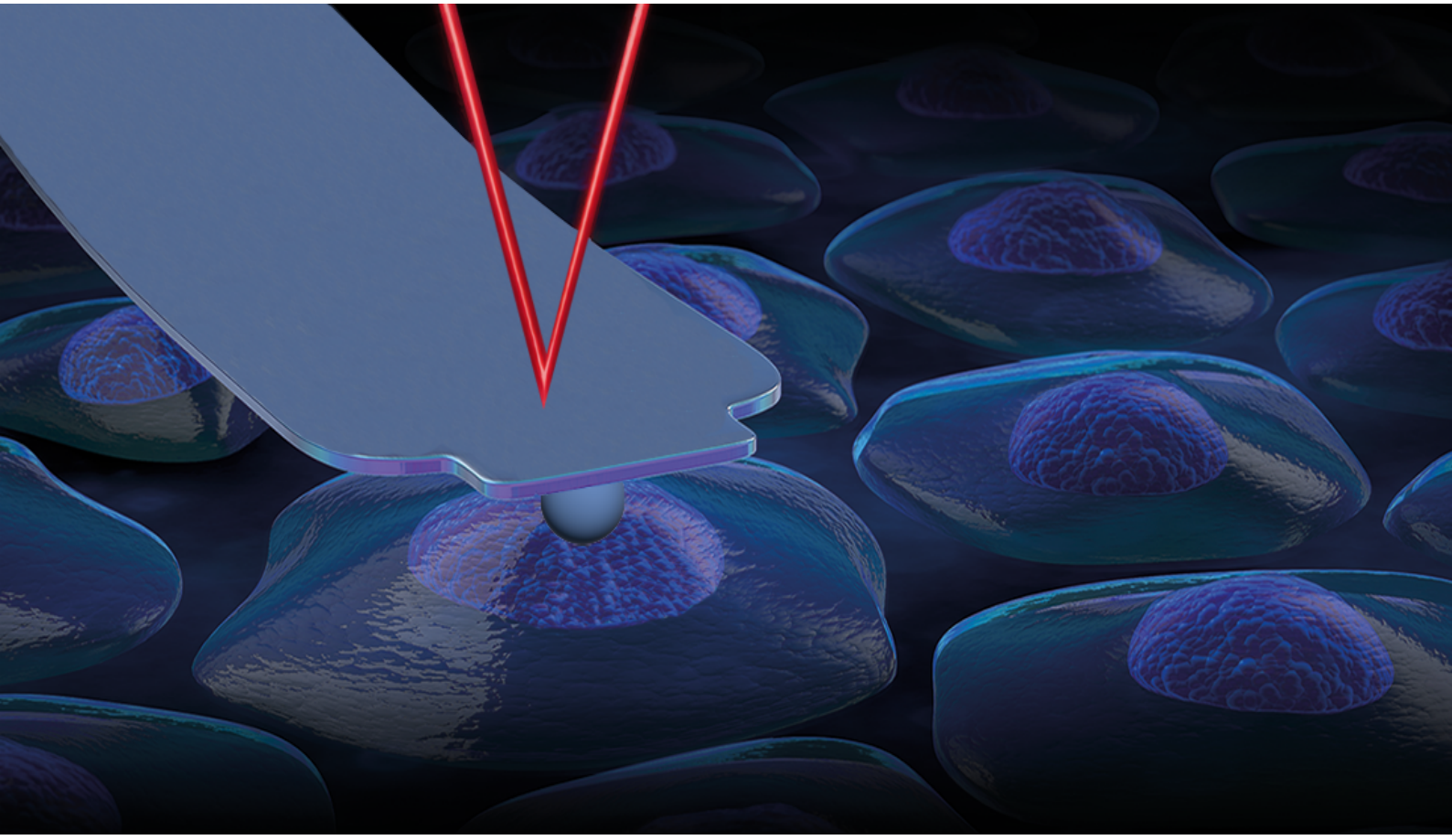

TU Delft Delft University of Technology

Challenge the future

Experimental Characterization of the Young's Modulus of MCF-7 Cancer Cells in Cell-Cell and Cell-Substrate Configurations using AFM

Master Thesis

by

Monique Nguyen

to obtain the degree of Master of Science
Delft University of Technology
to be defended publicly on Wednesday December 11, 2024 at 09:00 AM.

Student number:	4751142
Project duration:	March, 2023 - December, 2024
Supervisors:	dr. M. K. Ghatkesar
	dr. ir. V. U. Shastri
External:	dr. P. Boukany

TU Delft

Abstract

Cancer metastasis, the spread of cancer cells from a primary tumor to distant organs, is the leading cause of cancer-related deaths. During metastasis, cancer cells undergo significant changes in their mechanical properties, including alterations in cell elasticity. Cancer cells generally exhibit higher elasticity than normal cells, a key feature that may contribute to their ability to migrate and invade other tissues. Although extensive research has focused on cell-substrate interactions, these studies do not fully replicate the physiological environment, where cells are frequently in direct contact with each other. In this study, Atomic Force Microscopy (AFM) in force spectroscopy mode, utilizing a micro-sized cantilever with a hemispherical tip, was used to quantify the Young's modulus (E) of MCF-7 breast cancer cells in two configurations: cell-substrate and cell-cell. The resulting force-indentation curves were analyzed and fitted to the Hertz contact model to determine the Young's modulus. The results showed that the Young's modulus in the cell-cell configuration was E_{cc} = 205.8 ± 50.88 Pa, while in the cell-substrate configuration, it was E_{cs} = 187.95 ± 78.26 Pa. These findings suggest that MCF-7 cells are slightly less elastic in the cell-cell configuration. This challenges the expectation of a more significant difference between the two configurations and highlights the importance of considering biological variability and experimental conditions when interpreting cell mechanical properties.

Introduction

Cancer metastasis, the spread of cancer cells from a primary tumor to distant organs, is responsible for over 90% of cancer-related deaths [1]. To successfully metastasize, cancer cells must navigate different microenvironments, overcome physical barriers, and engage in various interactions [2]. These processes are influenced by mechanical forces acting on and within the cells, a key focus of mechanobiology, the field that investigates how cells perceive and respond to mechanical stimuli [3].

Scientific research has shown that cancer cells often exhibit altered mechanical properties compared to non-cancerous cells [4–6]. Specifically, cancer cells tend to have increased elasticity, as evidenced by a lower Young's modulus (E) compared to healthy cells [7]. This altered elasticity is believed to contribute to the cells' invasive and metastatic behavior, making the study of their mechanical properties crucial for understanding metastasis.

Biophysical techniques, such as Atomic Force Microscopy (AFM), enables the study of cellular mechanics under physiological conditions [8]. Among these, AFM operating in force spectroscopy mode is particularly well-suited for studying cell mechanics. This technique has led to a deeper understanding of many biological and physical processes down to the single-molecule level, offering nanometer resolution, piconewton sensitivity, and the ability to measure biological samples under physiological conditions, thus enhancing the biological relevance of the measurements [9–11]but. Force spectroscopy mode operates by measuring the repulsive or attractive forces between the micro-sized cantilever tip and the sample surface, with laser tracking of the cantilever deflection as its tip interacts with the sample.

While most research on cancer cell elasticity has focused on cell-substrate interactions, the role of cell-cell interactions in cancer progression has remained underexplored. However, cancer cells within tumors interact with each other and their surrounding microenvironment, with mechanical properties playing a crucial role in the metastatic process. By investigating the elasticity of cancer cells in a cell-cell configuration, this research aims to address a significant gap in the literature, offering new insights into the mechanical behaviors of cancer cells in more physiologically relevant conditions, such as those found in the tumor microenvironment (TME).

In this study, the Young's modulus of the MCF-7 human breast cancer cell line was quantified in both cell-to-cell and cell-substrate configurations using AFM in force spectroscopy mode. To reliably characterize the elastic properties, a reproducible method was essential. The AFM indentation method was employed, wherein a cantilever with a hemispherical tip was pressed into MCF-7 cells in both configurations. During this process, the cantilever's deflection and position were continuously measured, generating force-distance curves. These curves were analyzed using JPK data processing software, which fits the data to the Hertz contact model. This model correlates the indentation depth and applied force to calculate the Young's modulus of the MCF-7 cells in both configurations.

This research represents an interdisciplinary collaboration between three departments at TU Delft: Precision and Microsystems Engineering (PME), Chemical Engineering, and Bionanoscience. The PME department is responsible for quantifying the elastic properties at the single-cell level, the primary objective of this research. The Chemical Engineering department will use this quantitative data to construct a model connecting cellular and tissue-level behaviors, while the Bionanoscience department will experimentally validate the model under various conditions. The overarching aim is to provide a biophysical perspective on tumor behavior, complementing existing biochemical knowledge and contributing to improved strategies for preventing and treating cancer metastasis.

The study is structured as follows: Part I presents an adapted literature review, providing essential background on cancer biology and experimental techniques for measuring cell mechanics, with a focus on AFM. It also includes a review of existing AFM-based elasticity measurements in cancer cells. The section concludes by identifying the research gap and formulating the research question. Part II details

the experimental research, including materials and methods for performing AFM indentation measurements, followed by the results, discussion, and conclusion. Finally, Part III contains the appendix, which provides supplementary materials relevant to the research.

Contents

I

Literature

1
Cancer biology

This chapter begins with an introduction to cancer biology, followed by an overview of the steps involved in cancer metastasis and the composition of the tumor microenvironment (TME).

1.1. Cancer

The human body is a complex organism composed of trillions of cells working together to maintain tissue structure and function [12]. Under normal conditions, cells undergo regulated division, supporting growth, repair, and the replacement of old or damaged cells [13]. This balance is crucial for sustaining the physiological functions of tissues and organs [14]. Cancer, however, is characterized by the uncontrolled division and proliferation of abnormal cells, disrupting this balance and interfering with normal physiological processes [15].

Cancer starts with DNA damage, known as mutations, occurring within cells (Figure 1.1A) [16]. Mutations affecting genes that regulate the cell cycle and DNA repair mechanisms disrupt the control of cell division [17, 18]. This disruption leads to an accumulation of DNA damage, often undetected, which eventually results in the formation of abnormal growths known as tumors (Figure 1.1B) [16]. Tumors can be categorized into two main types: benign and malignant [19]. Benign tumors generally remain localized at their original site without invading surrounding tissues, often posing minimal threat to the overall health of the individual. In contrast, malignant tumors, or cancers, have the ability to invade nearby tissues and spread to distant parts of the body through a process known as metastasis (Figure 1.1C).

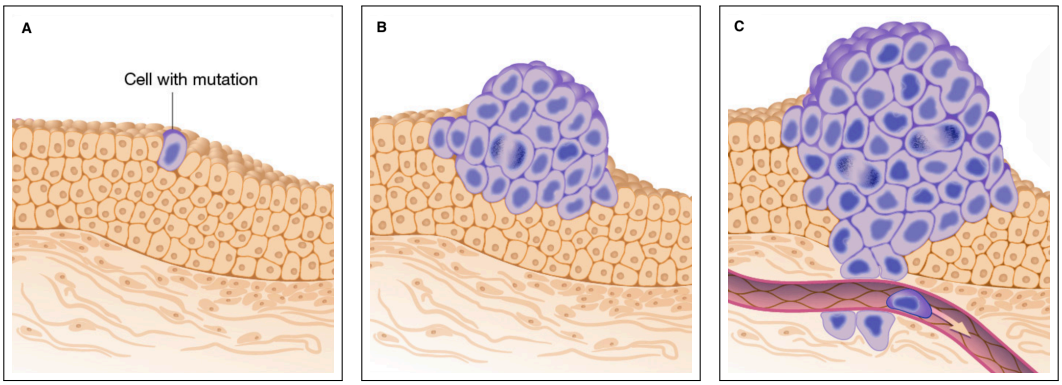

Figure 1.1: Cancer development (A) Cancer starts when a single cell acquires a mutation that allows it to divide and multiply uncontrollably **(B)** As these mutated cells continue to divide and accumulate more mutations, they can form a mass of abnormal cells (tumor) at the primary site. **(C)** Some of these cells may acquire the ability to invade nearby tissues and, in some cases, spread to other parts of the body, a process known as metastasis. [20]

1.2. Cancer Metastasis

Metastasis is a complex and multistep process in which cancer cells spread from the primary tumor site, migrate through various microenvironments, and establish new tumors in other parts of the body [1]. The metastatic cascade (Figure 1.2) begins with the accumulation of cells that divide and multiply uncontrollably, leading to the formation of the primary tumor. As the primary tumor grows, it requires more oxygen, which triggers the formation of new blood vessels (vascularization) [21]. At the same time, some tumor cells detach from the primary tumor, invade nearby tissue, and enter the blood vessels in a process known as intravasation [22]. These tumor cells become circulating tumor cells (CTCs), circulating through the vascular system [23]. Some CTCs adhere to vessel walls and undergo extravasation, exiting the bloodstream [24]. Once outside the vessels, they can form secondary tumors. The formation and growth of secondary tumors depend on the physical interactions and mechanical forces between cancer cells and the tumor microenvironment (TME).

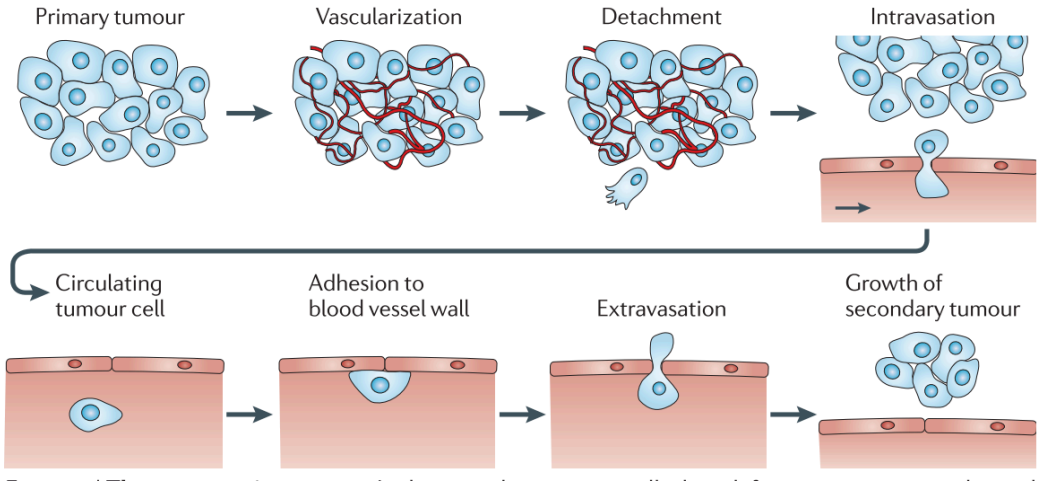

Figure 1.2: The metastatic process begins when a cancer cell detaches from the vascularized primary tumor, penetrates the surrounding tissue, enters a nearby blood vessel (intravasation), and circulates through the vascular system. Upon reaching a small blood vessel at a distant site, the cancer cell can adhere to the vessel wall. After adhering to the vessel wall, the cancer cell penetrates the blood vessel wall (extravasation) and enters the surrounding tissue, where it can establish a secondary tumor. [1]

The complex and multistep process of metastasis presents numerous mechanical challenges for cancer cells. At each stage of the metastatic cascade, cancer cells encounter various microenvironments that demand demand specific mechanical properties for successful progression. For instance, efficient migration requires cells to exhibit optimal elasticity and force generation [1]. Furthermore, During intravasation, cancer cells must enter the bloodstream from the primary tumor site, which involves squeezing between the endothelial cells lining the blood vessel walls. This process requires cells to undergo significant deformation to penetrate the tight junctions between endothelial cells [25]. In summary, cancer cells must rapidly adjust their cellular structure and mechanics to adapt to these biophysical demands.

Understanding how cancer cells overcome these mechanical challenges and adapt their properties will enhance our understanding of metastasis progression. In addition to these mechanical challenges, the interaction of cancer cells with their surrounding microenvironment is a crucial aspect of metastasis. The following section will delve into the complexities of the tumor microenvironment (TME) and its significant impact on cancer cell behavior and progression.

1.3. Tumor Microenvironment (TME)

Cancer cells are not the only components of tumor tissue, it also contains non-cancerous cells and non-cellular elements, which can make up to 50% of its composition [26]. This cellular environment, known as the tumor microenvironment (TME), is shown in Figure 2.3. The TME consists of various cell types, including host cells such as blood vessels, immune cells, and fibroblasts, as well as non-cellular components like the extracellular matrix (ECM) and signaling molecules [27–29]. Within the TME, cancer cells interact with these components and with each other, creating a complex and dynamic environment that significantly influences the progression of the disease [30, 31]. Studying these interactions is crucial, as research demonstrates that the TME is not merely a passive observer but an active participant in cancer progression [32].

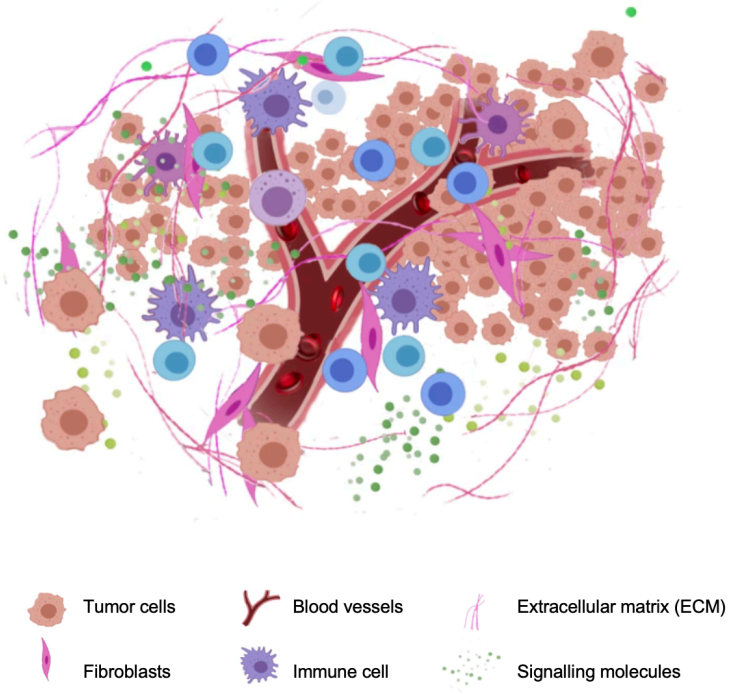

Figure 1.3: The Tumor Microenvironment (TME) Within a tumor, cancer cells are surrounded by immune cells, fibroblasts, signaling molecules, extracellular matrix (ECM), and blood vessels. Cancer cells can modify the microenvironment, affecting cancer growth and spread. [33]

Cancer cells possess the ability to modify and recruit various cell types within the tumor microenvironment (TME), including fibroblasts, immune cells, and vascular cells, through the release of specific substances such as growth factors and signaling molecules [34]. These recruited cells actively contribute to maintaining the TME by altering non-cancerous cells, reshaping tissue structures, and modulating the immune system [35]. This dynamic interaction creates a more supportive environment for the survival, growth, and progression of cancer cells.

2
Cell components and Elasticity

This chapter starts with an overview of the cellular components, with a particular focus on their elasticity.

2.1. Cell structure

A cell is the fundamental structural and functional unit of life, acting as the core building block of all living organisms [36]. A typical cell consists of several key components, including the cell membrane, cytoplasm, nucleus, cytoskeleton, and various organelles [37]. Cells are broadly classified into two types based on the presence or absence of a nucleus. Eukaryotic cells, found in humans, animals, and plants, contain a nucleus and typically range in size from tens of microns [38, 39]. In contrast, prokaryotic cells, present in certain bacteria and blue-green algae, lack a defined nucleus, with their genetic material spread throughout the cytoplasm [40]. The complex microstructure of a typical eukaryotic cell is schematically illustrated in Figure 2.1.

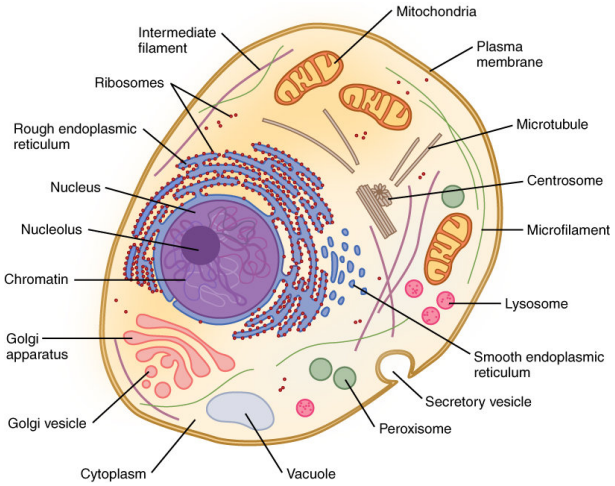

Figure 2.1: Schematic representation of a typical eukaryotic cell and its organelles. [41]

The mechanical behavior of cells is primarily influenced by four key components: the cell membrane, cytoplasm, nucleus, and cytoskeleton [42]:

- **Cell membrane**: The cell membrane, the outermost layer of the cell, has a thickness of 7-10 nm [43]. Its primary function is to regulate the movement of substances into and out of the cell, maintaining cellular integrity and communication.
- **Cytoplasm** The cytoplasm is a translucent, colloidal, and granular substance enclosed by the cell membrane, excluding the nucleus. Composed of approximately 80% water [44], it houses specialized organelles such as the Golgi apparatus, mitochondria, endoplasmic reticulum, ribosomes, and others. Each organelle plays a critical role in maintaining cellular functions and vitality [42].
- **Nucleus** The nucleus serves as the control center of the cell, orchestrating genetic and metabolic activities. It comprises four main components: the nuclear membrane, nucleolus, nuclear matrix, and chromatin. The chromatin, in particular, holds the genetic material essential for the cell's functioning and replication [45].

- **Cytoskeleton** The cytoskeleton is a dynamic network of biopolymers located in the cytoplasm that determines the cell's shape, structure, and mechanical properties. It plays a critical role in maintaining cell morphology, resisting external forces, and facilitating essential processes such as intracellular transport, division, and motility. The primary components of the cytoskeleton are microfilaments, microtubules, and intermediate filaments [46].

In summary, the mechanical behavior of cells is shaped by the combined actions of the cell membrane, cytoplasm, nucleus, and cytoskeleton. Each component contributes uniquely to the cell's structural integrity and functionality. Together, these components form a cohesive system that enables cells to adapt to their environments, perform specialized functions, and respond to mechanical stimuli, highlighting the intricate relationship between cellular structure and mechanics.

2.2. Cell elasticity

The mechanical properties of cells, such as elasticity, adhesion, and viscosity, are critical in determining how cells move, deform, interact, and respond to mechanical forces [39]. These properties are often altered in various diseases, with cancer being a notable example [47]. A study by Lekka et al. demonstrated that, regardless of the cancer type, cancer cells consistently exhibit a lower Young's modulus, indicating increased elasticity [7]. This observation highlights the significance of understanding cell elasticity, particularly in the context of cancer. The remainder of this section will focus specifically on the elasticity of cells.

Cell elasticity, or the Young's modulus (E) or elastic modulus, plays a vital role in various biological processes, including tumor progression [48]. In this study, the term 'elastic modulus' is used to describe a material's elasticity, with the quantified value referred to as 'Young's modulus (E)', the specific measure of elasticity for the sample under the tested conditions. Elastic modulus is defined as the resistance of an elastic body to deformation when an applied force is introduced [7]. For eukaryotic cells, the elastic modulus typically ranges from a few hundred pascals (Pa) to tens of kilopascals (kPa) [39].

The observed changes in the elasticity of cancer cells are closely linked to the remodeling of the cytoskeleton [7]. The cytoskeleton is a dynamic network of biopolymers composed of microfilaments, microtubules, and intermediate filaments [49]. These biopolymers provide structural stability, enable mechanical communication, and facilitate motility [46]. The arrangement of these cytoskeletal components significantly influences the cell's overall elasticity because these components have different elasticity properties, which play distinct roles in cell deformation and resistant to forces. To further understand the influence of the cytoskeleton on cell elasticity, the individual contributions of its components have been examined:

- **Microfilaments** also known as actin filaments, are composed of several thin actin chains that twist around each other, forming a structure resembling a double helix with a diameter between 6-8 nm and a Young's modulus ranging from 1.3-2.5 GPa [11]. They are primarily concentrated just beneath the cell membrane, where they provide support to the cell and assist in maintaining its shape.
- **Microtubules** are the stiffest of the biopolymers. They are hollow cylinders primarily composed of polymers of alpha (α) and beta (β) tubulin with an inner diameter of 14 nm, an outer diameter of 25 nm, and a Young's modulus of 1.9 GPa [11]. The main functions of microtubules are maintaining the cell's shape, holding organelles in place, and facilitating their movement within the cell.
- **Intermediate filaments** (IFs) are compsed of diverse protein subunits, typically exhibiting an average diameter of 10 nm and a Young's modulus ranging from 1-5 GPa [11]. They have a dense and stiff structure that restricts their ability to undergo dynamic remodeling. Consequently, they play a lesser role in cell movement and migration compared to actin and microtubules. Their primary function is to provide essential structural support for cells and contribute to the maintenance of cell shape and integrity.

Several studies have explored the roles of the structural biopolymers within the cytoskeleton in cancer cells [50–53]. These studies consistently show that actin filaments, known for their dynamic

properties, play a central role in determining the mechanical behavior of cells. For example, Xu et al. found denser, well-aligned F-actin with longer stress fibers in non-malignant IOSE (Immortalized Ovarian Surface Epithelium) cells, which serve as the counterpart to ovarian cancer cells [5]. In contrast, ovarian cancer cells exhibited reduced levels of F-actin filaments and stress fibers, particularly near the cell membrane [6, 54]. Additionally, the microtubule network in cancer cells was found to be sparse with significant voids [55]. These alterations contribute to a softer and more elastic cell structure, enabling cancer cells to undergo rapid shape changes and navigate through narrow spaces, a key feature for metastasis.

Current understanding reveals that cells are complex and heterogeneous, composed of various proteins, filaments, subcellular structures, and organelles, each of which uniquely influences cell elasticity, as illustrated in Figure 2.2. For example, the glycocalyx, the outermost layer of the cell, is a flexible structure with a Young's modulus ranging from 10–100 kPa [56]. Beneath the glycocalyx lies the cell membrane, a delicate structure under low tension, influenced by the underlying actomyosin cortex, which is considerably more rigid, with a Young's modulus ranging from 10–100 kPa [56]. Additionally, the rigid filamentous structures of the cytoskeleton have a Young's modulus of approximately 0.1–1 kPa [57], while the nucleus has a Young's modulus ranging from 1–10 kPa [45]. This variation in elasticity across different parts of the cell emphasizes that each region contributes differently to the overall mechanical behavior, and the overall elasticity may vary depending on which part is measured.

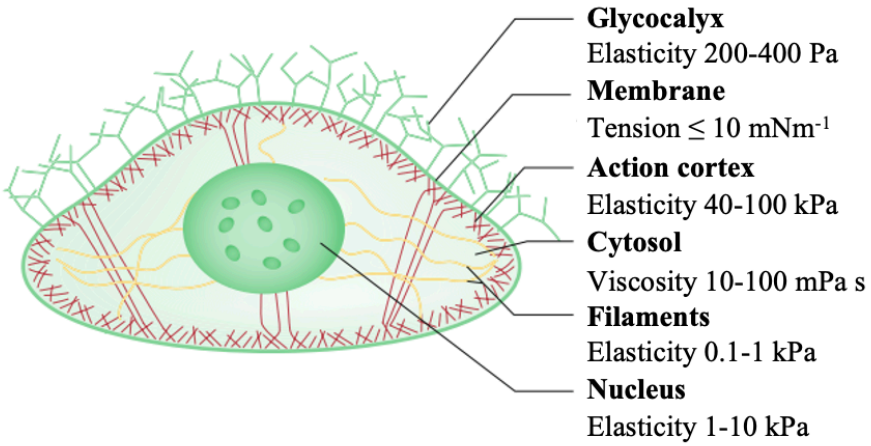

Figure 2.2: Schematic representation of a typical cell highlighting the mechanical characteristics of its internal structures and compartments. [10]

3

Experimental Techniques for measuring cell mechanics

This chapter provides a brief overview of the experimental techniques used to measure cell mechanics, the study of the mechanical properties and behaviors of cells, such as elasticity, with a specific focus on Atomic Force Microscopy (AFM).

3.1. Measurement methods

Researchers have extensively explored cell mechanics using various experimental methods, which can be broadly classified into two categories: force-application techniques and force-sensing techniques [58]. Force-application techniques involve applying a known force or stress to the cell, such as by indenting or stretching its surface, and subsequently measuring the resulting deformation or biochemical response [59]. In contrast, force-sensing techniques involve seeding cells onto deformable substrates or structures, enabling the measurement of traction forces generated by the cells [58].

The selection of a technique depends on the research objectives and the specific mechanical properties being studied. Force-application techniques are widely used to determine a cell's material properties. These techniques can target either the entire cell or specific localized regions. The most commonly used force-application techniques are illustrated in Figure 3.1. Techniques A–D evaluate the cell's response to forces applied across its entire surface, while techniques E–F focus on the response to localized forces.

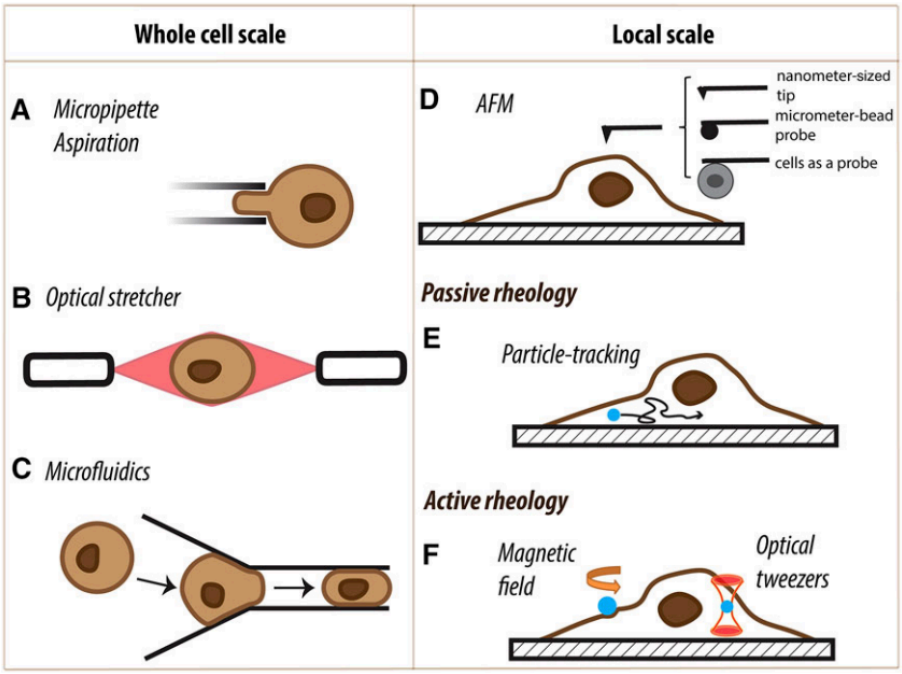

Figure 3.1: Cell mechanics techniques whole cell scale **(left)** and local scale **(right) A.** Miropipette aspiration (MA) **B.** Optical stretcher **C.** Microfluidics (MT) **D.** Atomic force microscopy (AFM) **E.** Passive rheology **F.** Active rheology [60]

Each technique offers distinct strengths and limitations, characterized by differences in spatial and temporal resolution, sensitivity, and throughput [61]. Although a comprehensive analysis of all these methods is beyond the scope of this chapter, their principles, advantages, and limitations have been extensively reviewed in previous studies [58, 62, 63].

Atomic Force Microscopy (AFM) was chosen as the primary technique for this research due to its unique advantages in studying cell mechanics. When operating in force spectroscopy mode, AFM provides high sensitivity (in pN) and spatial resolution (in nN), enabling precise measurements of mechanical properties at the nanoscale [64]. Additionally, AFM allows for measurements under conditions that closely mimic the physiological environment of biological samples, ensuring that the results reflect the natural behavior of cells [64]. AFM has been successfully used in previous studies to quantify the elastic properties of cells, as will be reviewed in Chapter 4, further supporting its suitability for this research. These features make AFM an ideal choice for investigating the elastic properties of cancer cells in both cell-cell and cell-substrate configurations. Since this research utilized AFM to estimate the elastic properties of cancer cells, the following section focuses on a detailed explanation of the AFM measurement technique.

3.2. Atomic Force Microscopy (AFM)

Atomic Force Microscopy (AFM) is a high-resolution surface characterization technique that has gained significant popularity for imaging and mechanically analyzing a broad range of biological samples [65]. The key components of the AFM system in force spectroscopy mode are shown in Figure 3.2. The AFM operates by using a tip, in this case a spherical tip, attached to a flexible cantilever that interacts with the sample, which in this example is a cell. As the tip indents the cell, the interaction forces cause the cantilever to deflect. This deflection is measured by a laser beam reflected off the back of the cantilever onto a photodetector. The force curves obtained from these experimental AFM measurements can be analyzed to determine the material properties of the sample.

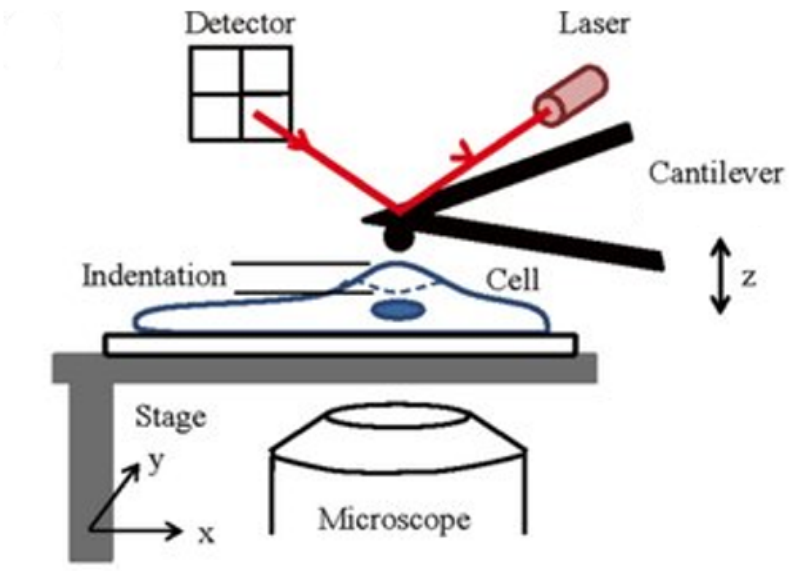

Figure 3.2: Schematic diagram of the main components of an AFM operating force spectroscopy mode including a cantilever with a colloidal tip at its free end, an optical detection system, and the piezoelectric scanners. [66]

The following section further elaborates on the main components of the AFM system:

1. **Scanning and positioning system** The scanning and position system utilizes piezoelectric scanners to achieve precise movement and positioning of both the sample and the cantilever. This system is crucial for ensuring accuracy in the AFM measurements [67].

2. **Cantilever** The cantilever is a fundamental component of the AFM as it holds the tip that makes direct contact with the sample surface. The cantilever functions as a flexible spring, measuring the interaction force through its deflection, which is then translated into a measurable signal. Commonly, cantilevers are rectangular or V-shaped and are made from materials such as silicon or silicon nitride [67].

   Key characteristics of the AFM probe include:

   a) **Spring constant (k)** The spring constant, denoted as k, represents the cantilever's stiffness and is vital for accurate force measurements. It affects both the deflection response and the forces exerted by the cantilever on the sample [68]. For cell mechanics studies, the spring constant typically ranges from 0.01 to 1.0 N/m [64]. To ensure precision, the cantilever's spring constant must be calibrated before measurements. Calibration is often performed using the AFM's built-in software, which applies thermal noise measurement. Without proper calibration, force measurements cannot be accurately quantified [69].

   b) **Geometry of the tip** The geometry of the AFM tip is crucial for determining the spatial resolution of the technique. Various tip shapes are available, including pyramidal, conical, cylindrical, spherical, and wedge-shaped designs [10]. Smaller tips, such as pyramidal ones, provide higher spatial resolution and are ideal for capturing fine structural details. In contrast, larger tips (for instance spherical) are better suited for obtaining more averaged surface representations. The choice of tip geometry is based on the specific research objectives and the desired level of detail.

3. **Optical detection system** The optical detection system includes a laser and a photodiode, which are used to measure the deflection of the cantilever. The laser beam is focused on the back of the cantilever above the tip, and its reflection is detected by the photodiode, which is divided into four quadrants. Normally, the laser beam is directed toward the center of the photodiode. However, when interaction forces cause the cantilever to deflect, the reflected beam shifts, leading to changes in the photocurrents recorded by the photodiode's quadrants [67].

3.2.1. Force spectroscopy mode

For cell mechanics experiments, AFM operates in force spectroscopy mode, conducting force-distance measurements by fixing the cantilever's lateral position while varying its Z-position [70]. This mode enables nanometer (nm) resolution and piconewton (pN) sensitivity, making AFM a highly precise and quantitative technique for studying cell mechanics [9].

During AFM force spectroscopy experiments, the cantilever tip moves vertically toward and away from the sample in two phases: approach and retraction. During the approach phase, the tip contacts the sample, creating a small indentation until the cantilever deflection reaches the predetermined setpoint value. The retraction phase begins as the cantilever moves away from the sample, initially maintaining contact due to adhesion forces, and continues until the tip fully disengages after a specified Z-length.

Throughout both phases, tip-sample interactions cause the cantilever to deflect. This deflection is detected by the photodetector as changes in voltage (V), which are converted into deflection values ($d = S \cdot V$) in nm using the sensitivity S (measured in nm/V) [71]. The deflection is then used to calculate the force using Hooke's law ($F = k_c \cdot (S \cdot V)$ where the force is the product of the deflection and the calibrated spring constant of the cantilever [72]. Throughout both phases, tip-sample interactions are measured continuously, generating a force-distance curve. In the resulting force-distance curve:

- The **x-axis** represents the displacement of the cantilever relative to its initial position.
- The **y-axis** represents the force acting on the tip of the cantilever calculated by combining the photodetector signal, sensitivity calibration, and cantilever spring constant via Hooke's Law.

The following description of a typical force-distance plot is based on the explanations provided by Park Systems [73]. Figure 3.3 illustrates a force-distance plot in air obtained from force spectroscopy data. The cycle begins at point A, where the tip is far from the sample, and no interactions are present. From point A to point B (the baseline), the tip approaches the sample, but the cantilever remains undeflected, and the force acting on the tip is essentially zero. At point B, referred to as the contact point, the tip makes contact with the sample in an event called snap-in. This occurs as the cantilever approaches the surface, and the attractive forces, becomes surpass the cantilever's spring constant, causing the tip to rapidly snap into contact with the surface.

Once contact is established, if the cantilever's stiffness exceeds the sample's elasticity, the tip acts as an indenter, causing a small deformation. This deformation provides insights into the sample's elastic properties, enabling the estimation of its Young's modulus. The indentation continues until the cantilever reaches a predetermined setpoint force, marked as point C on the curve (highlighted with a blue circle).

From point C to point E, the cantilever is retracts from the sample's surface. However, between points D and E the tip and sample remain in contact due to adhesion forces. At point E, the stiffness of the cantilever overcomes these adhesion forces, leading to pull-off, where the tip detaches from the surface. This experimental process can be repeated at multiple locations on the sample or at the same site to gather comprehensive data on the sample's mechanical properties.

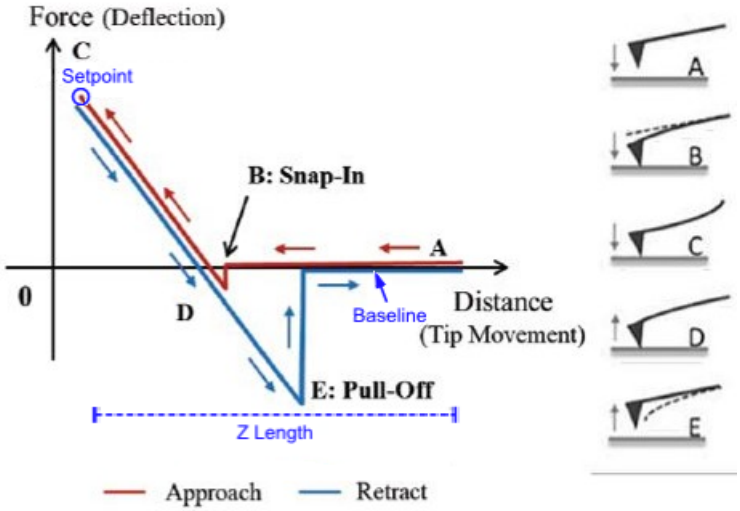

Figure 3.3: Plot showing the approach (red) and retraction (blue) curves of a conventional force-distance graph, with the cantilever force plotted against the piezo position. On the right, the positions of the pyramidal probe and the flat sample surface on the piezo are illustrated for various interaction points along the curve, labeled A–E [73]

Since the detector signal reflects both sample deformation and cantilever deflection, it is necessary to convert the force-distance curve into a force-indentation curve. This transformation accounts for the actual indentation depth of the tip relative to the sample surface, as the measured distance (Z) includes both the cantilever's movement and the sample's deformation. The formula used for this transformation is: $\delta = Z - d$, where δ is the indentation depth of the tip relative to the sample surface, Z is the total displacement of the cantilever (which includes both the sample deformation and cantilever deflection) and d is the deflection of the cantilever, representing its movement due to forces acting on the tip [71]. By subtracting the cantilever deflection d from the total displacement Z, the true indentation depth δ is obtained, reflecting only the deformation of the sample and not the cantilever's movement. This force-indentation curve is crucial for accurately determining the mechanical properties of the sample, including its Young's modulus.

To calculate the Young's modulus from this data, the geometry of the tip-sample contact must be considered, along with an appropriate contact mechanics model, which will be discussed in the following section.

3.3. Contact models: Hertz Model

To determine the Young's modulus, elastic continuum theories, referred to as contact models in this study, are used to describe the mechanical behavior of materials during contact interactions [10]. These models are utilized to quantify material properties, such as the elastic modulus, based on AFM force-distance measurements.

The most commonly used models are the Hertz, Johnson–Kendall–Roberts (JKR), and Derjaguin–Müller–Toporov (DMT) models [74–76], each with different assumptions and applicability. The Hertz model is valid only when the adhesion force is much smaller than the maximum load. The JKR model is suitable for soft samples with significant adhesion and large tips, while the DMT model is more appropriate for stiff samples with small adhesion and small tips. Furthermore, the Hertz model neglects sample adhesion, whereas the DMT and JKR models account for adhesion both inside and outside the contact area [10].

However, all these models assume that the sample is purely elastic, lacks substructure, and extends infinitely [10]. Experimentally, these assumptions imply that the applied strain should not exceed 20%, blunted tips should be used, indentation should involve less than 10% of the sample thickness, the indentation area should be small relative to the sample dimensions, and normal loading (perpendicular to the sample surface) is assumed [10]. Each model is suited for specific indenter geometries and sample properties. Therefore, indenters are typically spheres, cones, or flat cylinders, as the contact mechanics for these geometries are well established [77]. Figure 3.4 illustrates the different probe geometries and assumptions for which each model is applicable.

The Hertz model is the most frequently used method for obtaining mechanical properties from AFM measurements [71]. It describes the deformation of two elastic spheres when they come into contact. This model can be generalized to describe the scenario where a sphere presses on a thick, elastic layer. However, a single cell is not a simple elastic layer, as it contains internal structures and compartments with varying mechanical properties [10].

Despite ongoing advancements in modeling the mechanical properties of individual cells, the Hertz model remains the most commonly used contact model for studying the elasticity of single cells [bronnen].

Model	Probe geometry	Force	Additional assumptions	Schematic representation
Hertz	Spherical	$F = E_{eff} \cdot \left[\left(a^2 + R_P^2\right) \cdot \ln\left(\frac{R_P + a}{R_P - a}\right) - 2aR_P\right]$ $\delta = \frac{a}{2} \ln \frac{R_P + a}{R_P - a}$	No surface forces	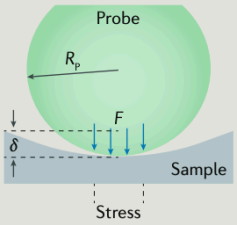
	Cylindrical	$F(\delta) = 2E_{eff} \cdot R_Z \delta$	Smooth punch profile (no edges)	–
	Conical (Sneddon model)	$F(\delta) = E_{eff} \cdot 2\tan(\theta)/\pi \cdot \delta^2$	Infinitely sharp probe	–
	Parabolic	$F(\delta) = E_{eff} \cdot \frac{4\sqrt{R_P}}{3} \delta^{\frac{3}{2}}$	$R_C > \delta$	–
	Blunted pyramidal	$F(\delta) = 2E_{eff} \cdot \left[\delta a - \frac{\sqrt{2}}{\pi} \frac{a^2}{\tan\theta}\left(\frac{\pi}{2} - \arcsin\frac{b}{a}\right) - \frac{a^3}{3R_P} + \sqrt{(a^2 - b^2)} \cdot \left(\frac{\sqrt{2}}{\pi} \frac{b}{\tan\theta} + \frac{a^2 - b^2}{3R_P}\right)\right]$	Cross section of pyramid modelled as a circle	–
Derjaguin–Müller–Toporov	Spherical	$F = F_{Hertz} - F_{det}$ $\delta = \frac{a}{2} \ln \frac{R_P + a}{R_P - a}$	• Long-range surface forces outside the contact area • Valid for stiff materials, small spheres and weak adhesion	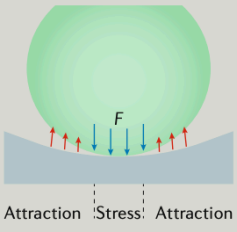
Johnson–Kendall–Roberts	Spherical approximated with a paraboloid	$F = F_{Hertz} - 4\sqrt{\frac{E_{eff} \cdot F_{det} a^3}{3R_P}}$ $\delta = \frac{a^2}{R_P} - 2\sqrt{\frac{F_{det} \cdot a}{3E_{eff} R_P}}$	• Short-range surface forces inside the contact area • Valid for compliant materials, large spheres and strong adhesion	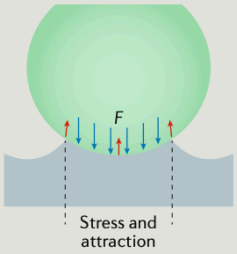

Figure 3.4: where δ, indentation depth; η, cytosolic viscosity; ν, Poisson ratio; ζ, pore size; a, contact radius; b, transition radius of a blunt probe; DP, poroelastic diffusion constant; E, Young's modulus; E_{eff} = E/(1 - ν^2)), effective Young's modulus; F, indenting force; F_{det}, detachment force; F_{Hertz}, force in the Hertz model; h, thickness of spherical shell; θ, semi-included angle of the probe; RC, radius of spherical cell; RP, radius of the indenting probe; RS, radius of spherical shell; RZ, radius of an indenting cylinder; TC, cortex tension. Image source: [10]

4

Review of AFM Methods for Measuring Cancer Cell Elasticity

This chapter reviews existing research, experimental findings, and methodologies for estimating the elastic properties of cancer cells using Atomic force microscopy (AFM) force spectroscopy.

4.1. Research review on Cancer Cell Elasticity

Before exploring existing research, it is essential to define the term normal. A normal cell originates from the same organ as its cancerous counterpart but is derived from healthy tissue. In the context of cell lines, normal cells retain the ability to proliferate but lack invasive or metastatic potential. These cells serve as a baseline for understanding typical cellular properties and behaviors. By comparing normal cells to their cancerous counterparts, variations or abnormalities indicative of disease can be identified.

As outlined earlier in this study, the term elastic modulus refers to a material's elasticity, while the quantified value, known as Young's modulus (E), represents the specific measure of elasticity under the tested conditions. Elastic modulus quantifies the resistance of an elastic body to deformation when subjected to an applied force. A higher Young's modulus corresponds to a material with greater resistance to deformation, indicating lower elasticity. In contrast, a lower Young's modulus reflects reduced resistance to deformation, signifying that the material is softer and more elastic.

Table 4.1 summarizes studies that employ AFM based single cell force spectroscopy (SCFS) elasticity measurements to distinguish cancerous cells from their normal counterparts.

Table 4.1: AFM-Based SCFS Elasticity Measurements in Distinguishing Cancerous Cells from Normal Cells. The cantilever column is organized as follows: the first row indicates the shape of the cantilever used, the second row provides the spring constants (k) of the cantilever in N/m, the third row specifies the tip geometry, the fourth row contains the approximation for the model, and the last row details the contact model. Adapted from [67]

Reference	Cantilever	Cell lines	E (kPa)	Key observations
Cross et al. [4]	V-shaped k = 0.02 N/m Not specified Conical Hertz	Benign mesothelial cells and metastatic adenocarcinoma cells	1.97$\pm$0.70 0.53$\pm$0.10	Within the same sample and when compared across samples from different patients, metastatic cancer cells are approximately $\sim$73+11 $\%$ softer than their benign counterparts.
Xu et al. [5]	V-shaped k = 0.03 N/m Sphere 4.7 μm Paraboloid Hertz	IOSE(55) OVCAR4(18) HEY(60) OVCAR3(20) HEYA8(59)	2.47$\pm$2.05 1.12$\pm$0.87 0.88$\pm$0.53 0.58$\pm$0.24 0.49$\pm$0.22	Analysis of non-malignant IOSE and four *ovarian* cancer cell lines reveal that cancer cells exhibit a lower mean elasticity compared to their non-malignant counterparts.

Continued on next page

Table 4.1 – continued from previous page

Reference	Cantilever	Cell lines	E (kPa)	Key observations
Li et al. [6]	V-shaped k = 0.01 N/m Sphere 4.5 μm Paraboloid Hertz	MCF-10A MCF-7	1.21 0.61	Malignant (MCF-7) breast cells were found to have an apparent Young's modulus significantly lower (1.4–1.8 times) than that of their non-malignant (MCF-10A).
Lekka et al. [78]	V-shaped k=0.05-0.1 N/m Pyramid Paraboloid Sneddon	Hu609 HCV29 Hu456 T24 BC3726	9.7$\pm$3.6 7.5$\pm$3.6 1.0$\pm$0.6 0.8$\pm$0.4 0.3$\pm$0.2	Normal cells ($\sim$ 10 kPa) are found to have an order of magnitude stiffer than cancer cells ($\sim$ 1 kPa) and this was attributed to the reorganization of the cytoskeleton. In comparing the Young's moduli, it is evident that cancerous cells are significantly more elastic than their normal counterparts.
Kwon et al. [79]	V-shaped k= not specified Conical Sneddon	MCF-10A MCF-7 T47D MDA-MB-231	9.8$\pm$2.89 5.0$\pm$1.62 4.9$\pm$1.07 9.0$\pm$1.53	Cell elasticity of breast cancer cells was approximately 30-40$\%$ lower compared to their normal counterparts.
Ramos et al. [80]	V-shaped k = 0.01 N/m Pyramid Conical Sneddon	HCV29 HTB-9 HT-1376 T24	16.0$\pm$0.9 3.0$\pm$0.1 5.2$\pm$0.1 2.9$\pm$0.5	All malignant bladder cells have Young's moduli about 2–3 times lower that those non-malignant cells.
Faria et al. [81]	V-shaped k = 0.06 N/m Pyramid Conical Hertz	BHP LNCaP PC-3.1	2.80$\pm$0.49 0.287$\pm$0.05 1.40$\pm$0.16	The benign BPH cells are less easily indented and, therefore, exhibit a higher Young's modulus than the tumorigenic LNCaP and PC-3 cells. However, it was expected that the highly invasive PC-3 cells would have a lower Young's modulus than the non-invasive LNCaP cells. Surprisingly, this was not the case.
Lekka et al. [7]	V-shaped k = 0.01 N/m Pyramid Conical Hertz	PZHPV-7 PC-3 Du145 LNCaP 184A MCF7 T47D	3.09$\pm$0.84 1.95$\pm$0.47 1.36$\pm$0.42 0.45$\pm$0.21 2.26$\pm$0.56 1.24$\pm$0.46 1.20$\pm$0.28	The Young's modulus of normal and cancerous cells from breast and prostate tissues varies depending on the type of cancer. For prostate cancer cells, the Young's modulus was lower than that of PZHPV-7 (normal) cells by 337$\%$, 57$\%$, and 85$\%$ for PC-3, Du145, and LNCaP cells, respectively. For breast cancer cells, the Young's modulus was lower than that of 184A (normal) cells by 53$\%$ and 60$\%$ for MCF7 and T47D cells, respectively.

Continued on next page

Table 4.1 – continued from previous page

Reference	Cantilever	Cell lines	E (kPa)	Key observations
Efremov et al. [82]	Rectangular k = 0.06 N/m Sphere 9 μm Paraboloid Hertz	Vero Du145	1.30$\pm$0.90 0.60$\pm$0.40	DU145 cancer cells exhibited significantly lower Young's moduli, approximately 40$\%$, compared to the normal Vero cells. The values obtained for DU145 cells, using cantilevers with attached microspheres, were lower than those reported by groups employing sharp cantilevers for force spectroscopy.

The reviewed studies provide critical insights into the elasticity differences between cancerous and normal cells, revealing consistent trends that highlight the significance of elastic modulus measurements in understanding cell mechanics. These studies demonstrate how AFM-based SCFS can quantify elastic modulus to distinguish cell types and identify disease-related mechanical properties.

Key experimental insights:

1. **Cancer cells are more elastic than normal cells**
   Across studies, cancerous cells consistently show lower Young's moduli compared to their normal counterparts, indicating a reduced resistance to deformation. This increased elasticity is linked to cytoskeletal reorganization, a key feature of cancer progression. For example, Lekka et al. found that cancer cells ($\sim$ 1 kPa) are approximately an order of magnitude more elastic than normal cells ($\sim$ 10 kPa) [78].

2. **Variability across cancer cell lines**
   While the general trend is clear, the degree of elasticity reduction varies among cell lines and cancer types, highlighting heterogeneity. For instance:

   - Li et al. reported that malignant breast MCF-7 cells are 1.4–1.8 times softer than non-malignant MCF-10A cells [6].
   - In contrast, Ramos et al observed that malignant bladder cells had Young's moduli 2–3 times lower than their non-malignant counterparts, which is a more substantial reduction in elasticity compared to the breast cancer cell lines. [80]
   - Faria et al. found unexpected behavior in prostate cancer cells, where more invasive PC-3 cells exhibited higher moduli than less invasive LNCaP cells [81].

3. **Cantilever and geometry tip selection influence results**
   The experimental setup, including cantilever shape, spring constant, and tip geometry, significantly affects measured elastic moduli. For example:

   - Smaller tips (for example pyramidal) leads to a more focused force, resulting in less deformation and a higher elastic modulus.
   - Conversely, a larger tip (for example spherical), as used by Efremov et al. spreads the force over a larger area, causing more deformation and a lower elastic modulus [82]. Emphasizing the importance of ensuring that all experiments are conducted under the same or very similar conditions so that results can be reliably compared.
   - The spring constant of the AFM cantilever (which controls how sensitive the cantilever is to force) is another important factor. If different spring constants are used, it can affect how the force is applied and measured, making it difficult to compare results from different experiments.

4. **Measurement location**
   Measurements are often performed above the nucleus in cell elasticity studies. Measuring above the nucleus provides insight into the overall elasticity of the cell, which often reflects underlying nuclear mechanics in addition to the cytoskeleton. The elastic properties of the cytoplasm can vary significantly depending on the distribution of organelles and other intracellular components, leading to greater variability in measurements. To ensure consistency and comparability, many studies standardize their measurements by targeting the nuclear region.

5. **Application of elastic modulus as a diagnostic marker**
   The consistent reduction in elastic modulus for cancerous cells supports its potential as a biomechanical marker for early cancer detection and monitoring. However, variations in experimental design and biological factors necessitate careful standardization.

AFM-based force spectroscopy studies demonstrate that elasticity measurements can effectively distinguish cancerous cells from normal ones. Variations in elastic modulus highlight changes in cancer cell mechanics and the cytoskeleton, aiding our understanding of disease progression. The findings confirm Young's modulus as a key biomechanical property, but future research should focus on standardizing methods for better data comparability and exploring cell-cell interactions for more comprehensive insights.

5
Research framework

This chapter outlines the identified research gap, formulates the main research question, and presents the hypothesis.

Research gap
Although extensive research has focused on quantifying the elastic modulus of cancer cells in cell-substrate interactions, there is limited exploration into cell-to-cell interactions. The mechanical properties of cancer cells, particularly their elasticity, are crucial for understanding their behavior in the tumor microenvironment (TME) more importantly in the metastatic process. Most studies have examined cancer cells adhering to rigid substrates, which does not fully replicate the physiological environment where cells are often in direct contact with one another. This gap in research leaves important questions regarding how intercellular interactions affect the mechanical properties of cancer cells. Investigating the elastic modulus in a cell-on-cell configuration may offer deeper insights into the mechanics of cancer cells and their role in disease progression.

Main research question
The identified research gap, along with the insights gained from the literature review, led to the formulation of the following main research question:

How does the Young's modulus of MCF-7 breast cancer cells in a cell-cell configuration compare to that in a cell-substrate configuration, and what differences in elasticity can be observed?

This study aims to quantify the elastic modulus of MCF-7 cells in a cell-substrate and cell-cell configuration to explore their elastic properties and gain a better understanding of intercellular interactions. The experimental setup and methodology developed to address this question will be discussed in Part II of this study.

Hypothesis
Based on the literature review, the following hypothesis is proposed: MCF-7 cells in a cell-cell configuration, where they interact with another soft cell, will exhibit a lower elastic modulus compared to cells seeded on stiffer substrates. These differences in elasticity may be linked to changes in cell morphology and cytoskeletal organization. Cells cultured on soft substrates tend to adopt a more rounded morphology, while those on stiffer substrates spread out and become flatter. This hypothesis assumes that the mechanical properties of cancer cells, including their elasticity, are influenced by intercellular interactions. When cells are in direct contact with neighboring cells, rather than adhering to a rigid substrate, their mechanical properties, including elasticity, may be altered.

II
Project

6
Experiment materials and method

This chapter outlines the experimental procedure, materials, and methods, along with the methodological approach, describing each step of the experiment.

6.1. Materials

6.1.1. Cell culture

MCF-7, a well-established human breast epithelial cancer cell line, was selected as the model for studying cancerous elastic cell behavior [83]. The cell line is non-invasive and has a lot of biophysical data, making it perfect for comparative analysis. The MCF-7 cells were cultured in the facility of the Chemical Engineering Department, under the supervision of Dr. Pouyan Boukany and his research team. The cells are routinely cultured in T-25 flasks (Sarstedt) using Dulbecco's Eagle Modified Medium (Gibco) supplemented with 10% fetal bovine serum (Gibco) and 1% antibiotic-antimycotic (Gibco - contains Pen/Strep + Amphotericin B). Cells were incubated at 37°C in a humidified atmosphere with 5% CO_2, and the medium was refreshed every 2-3 days until the cells reached approximately 80% confluence. For the experiment, cells were seeded at a density of 2.0×10^5 cells per 34 mm petri dish and incubated overnight.

Figure 6.1 shows an image of MCF-7 cells cultured in the petri dish, taken prior to performing the AFM experiments. The image shows a typical adherent MCF-7 cell exhibiting a flat, spread morphology with well-defined borders, characteristic of cells grown on a substrate.

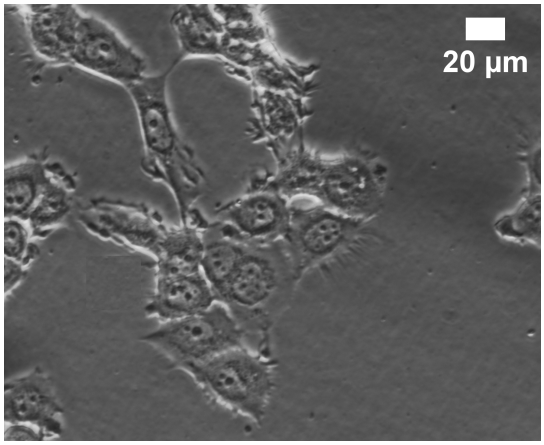

Figure 6.1: AFM topograpy image of MCF-7 cells captured in one of the collected petri dishes using a 40X lens, prior to performing the AFM experiment.

The morphological properties of MCF-7 cells depend on their culture conditions and stage of cell culture. Factors such as substrate stiffness, confluence, and growth environment can influence their length and height. Cells cultured on stiffer substrates tend to spread more, which can result in increased length and reduced height. In contrast, cells grown on softer substrates may adopt a more rounded or less elongated shape, leading to shorter lengths and greater heights [84]. Cultured MCF-7 cells typically have an average length of 20–25 μm [85]. Gil et al. reported that MCF-7 cells cultured on stiffer substrates (4.1–17.3 kPa) exhibited an average height of approximately 6 μm, whereas those grown on 100 Pa gels displayed significantly greater heights, reaching up to 10 μm [84].

6.1.2. Polyacrylamide (PAM) Hydrogel

For this study, easy-coat polyacrylamide (PAM) hydrogels, purchased from Matrigen were used [86]. These hydrogels, with a well-defined Young's modulus of 25 kPa, were provided in 35 mm Petrisoft (plastic-bottom) dishes to verify the experimental measurement and data analysis process.

6.2. Experimental equipment

6.2.1. AFM

AFM experiments were conducted using the JPK NanoWizard 4 AFM system in force spectroscopy contact mode [87]. The AFM system is optimized for performing experiments on samples in a liquid environment and equipped with a petri dish heater that maintained a constant temperature of 37°C to keep the cells viable throughout the experiments.

6.2.2. Cantilever

The micro-sized AFM cantilever, model type SAA-SPH-5UM, from Bruker was selected for the experimental measurements, SEM image of the cantilever is shown in Figure 6.2A [88]. This cantilever features a hemispherical tip that transitions into a cylindrical profile, as illustrated in Figure 6.2B. According to the manufacturer, it has a nominal spring constant of 0.25 N/m, a tip radius of 5 µm, and cantilever dimensions of 115 µm in length and 15 µm in width [88].

Given the expected elastic modulus of the cells, ranging from hundreds of Pascals (Pa) to several kilopascals (kPa), a cantilever with a nominal spring constant of 0.25 N/m is well-suited for these measurements. The hemispherical tip distributes force more evenly across the cell's surface, ensuring a more accurate representation of the cell's elastic properties. To quantify the elastic modulus, the Hertz contact model is applied, which is typically used for spherical tips and serves as an appropriate approximation for a hemispherical tip. This model allows for a straightforward calculation of the elastic modulus by relating the applied force, indentation depth, and contact area.

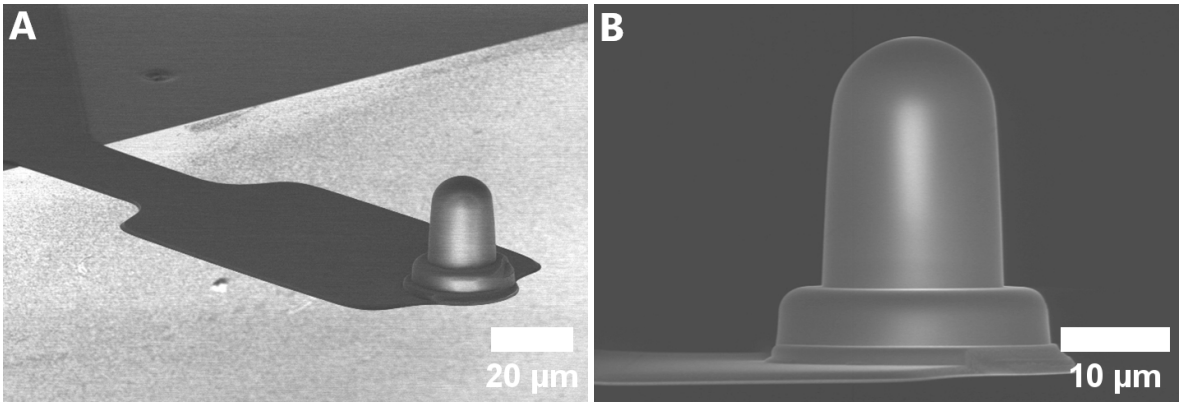

Figure 6.2: SEM images of the micro-sized cantilever with the hemispherical tip (SAA-SPH-5UM) - **(A)** Cantilever specification **(B)** Tip specification [88]

6.3. Experimental procedure for AFM force spectroscopy on cells

The experiment aimed to to obtain force-distance curves from MCF-7 cancer cells in two configurations: cell-substrate and cell-cell using AFM force spectroscopy. The procedure for conducting AFM force spectroscopy indentation measurements on the MCF-7 cell configurations is outlined in the following steps:

1. **Cell handling protocol**
    a) On the day of the experiment, four petri dishes containing cells in culture medium were collected from the Chemical Engineering Department of TuDelft. All containers were tightly sealed with parafilm to prevent spills during transportation.
    b) The sealed containers were then transported to the MNE laboratory of TuDelft where they were opened on the sample preparation table. The parafilm was removed, and the petri dishes were placed on a 37°C hotplate within an incubator to maintain cell viability until they were used in the measurements.
    c) One of the petri dishes was then removed from the incubator and placed onto the sample holder, which was equipped with a heater set to maintain the cells at physiological temperature (37°C) throughout the entire experiment.
2. **Set up the cnatilever and optical detection system**
    a) The cantilever (SAA-SPH-5UM) probe was mounted onto the cantilever holder, which was then locked in the AFM head. The AFM head was subsequently positioned onto the stage where the sample was located.
    b) The laser spot was aligned onto the cantilever and the mirror angle was adjusted until the reflected laser beam was centered on the photodiode. At zero deflection, the reflected laser spot must be precisely aligned with the center of the detector to achieve maximum sensitivity and optimal force control.
3. **Selection of feedback and measurement mode of the AFM**
    a) Once the sample was mounted and the cantilever aligned, the feedback mode and measurement mode were selected in the JPK SPM software. For the feedback control the ”Contact mode” was chosen, using the direct deflection of the cantilever as the feedback signal. For the measurement mode, ”Force Spectroscopy” was selected, which performs force-distance measurements.
4. **Cantilever calibration with the contact-free method**
    a) The cantilever properties (length = 115 µm and width = 15 µm) were entered in the calibration manager settings. The enivronment must be selected, the settings provide Air and Water for environment with corresponding density and viscosity, both of these change with temperature. The temperature was set to 37°C and the predefined environment (water) was selected with the corresponding density and viscosity.
    b) The cantilever was then calibrated: a quick and automatic thermal noise measurement was then performed. It is important to note that the cantilever calibration was performed in the cell culture medium to ensure that the measurements accurately reflect the conditions under which the cantilever will interact with the sample.

5. **Pick out location for indentation and automatic approach**

   a) Once the cantilever was calibrated, a location for indentation was selected on the Petri dish. For cell-substrate measurements, the cantilever was aligned above a single cell on the dish. For cell-cell measurements, the cantilever was directed toward two cells on top of each other. It is crucial to align the cantilever directly above the nucleus of the cell, whether in the cell-substrate or cell-cell configuration, to ensure accurate measurements.
   item Figure 6.3 shows the schematic of the AFM setup for the indentation experiments. Figure 6.3A represents the cell-substrate configuration, while Figure 6.3B illustrates the cell-cell configuration.

   b) The automatic approach was initiated, where the cantilever was moved towards the sample surface using the vertical deflection signal as feedback. At each step, the z-piezo extended, and the vertical deflection signal was monitored. If no change in deflection was observed, it indicated that the surface had not yet been reached. In this case, the piezo retracted, and the stepper motors move the AFM head closer to the sample. This process continued until the surface was detected. Once the approach was successfully completed, the system was ready for measurements.

6. **AFM indentation measurements on cells**

   a) The following parameters must be defined before starting the measurements: setpoint, indentation speed, and Z-length. The setpoint value represents the force applied to the sample. The indentation speed refers to the velocity of the cantilever, and the Z-length defines the range of the force curve.

   b) Perform AFM indentation measurements to obtain force curves. At each location, collect a minimum of five force curves before moving to another cell.

   c) Repeat steps 5 and 6 to gather a comprehensive dataset for both cell-substrate and cell-cell configurations.

In summary, AFM indentation measurements were systematically conducted over multiple days to ensure consistent data collection from different MCF-7 cells cultured under identical conditions. A minimum of five force curves were obtained at each location, providing a comprehensive dataset for analyzing cell elasticity.

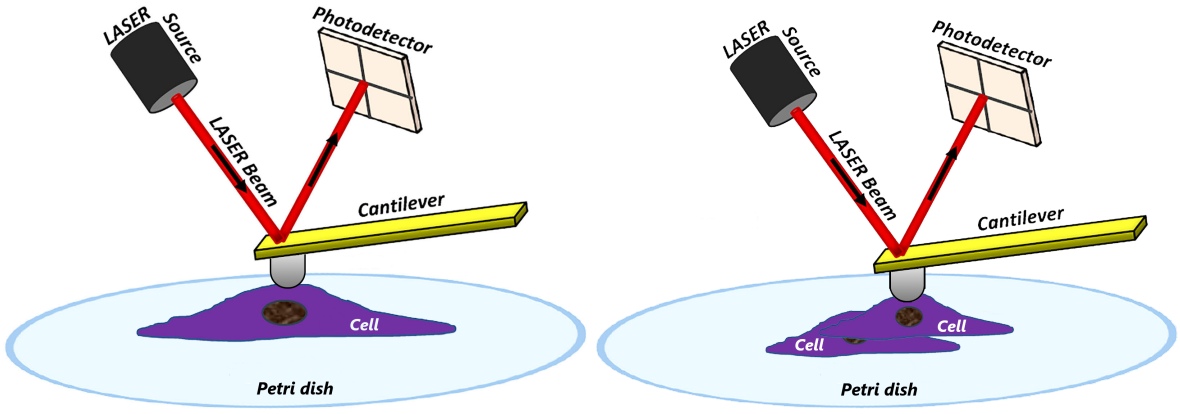

Figure 6.3: Schematic of AFM indentation measurements Illustration of the measurement setup for two configurations **(A)** AFM system probing the cell-substrate configuration and **(B)** AFM system probing the cell-cell configuration. Adapted from [89]

7

Data Analysis for quantifying Young's Modulus

This chapter focuses on analyzing force curve data obtained from atomic force microscopy (AFM) measurements to quantify the elastic modulus, specifically reported as Young's modulus.

7.1. Pre-processing raw data

All force curves were independently processed using JPK data processing software [87]. The first step was to identify and select analyzable force curves from the raw data, while non-analyzable curves were discarded. Analyzable force curves are characterized by smooth approach and retraction profiles, with a clear zero-force region (baseline) that allows for easy contact point determination.

An example of an analyzable force curve is shown in Figure 7.1A. In contrast, Figure 7.1B shows a force curve with drift in both the approach and retraction profiles, making it difficult to observe the true interaction between the probe and the sample. This figure also illustrates a force curve where the zero-force region (baseline) and the contact region are not clearly distinguishable, making it challenging to determine the contact point accurately. Proper identification of the contact point is essential for distinguishing true surface contact from noise or drift, which is crucial for accurate fitting with the Hertz contact model.

After identifying and selecting analyzable force curves, they are further processed using JPK data analysis software [87]. The software performs specific force curve operations to extract the Young's modulus.

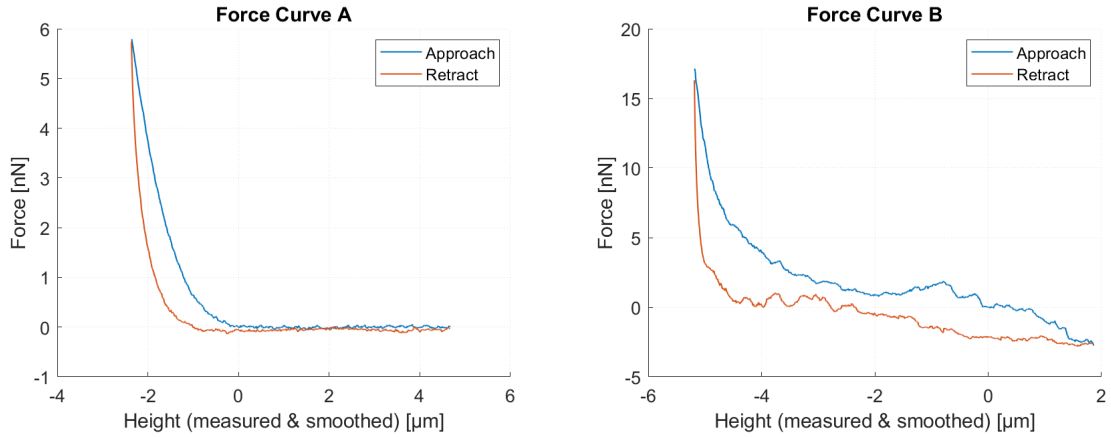

Figure 7.1: Force curves including both analyzable and non-analyzable examples obtained during measurements on single cell-petri dish - **(A)** An analyzable force curve displaying a smooth approach and retract profile with a well-defined baseline **(B)** A non-analyzable force curve with drift in approach and retract profile, with no clear distinction between the zero-force region and the contact region.

7.2. Force curve processing operations

The force curves obtained from AFM indentation measurements consist of an approach curve and a retraction curve. In this study, all analyses were performed on the approach curve for fitting with the Hertz model to calculate the elastic modulus. This decision was based on two primary considerations: 1) The approach curve allows for a more precise identification of the contact point, which marks the start of the elastic region described by the Hertz model. Accurate identification of this point is critical, as errors in its estimation can result in significant inaccuracies in the calculated elastic modulus. 2) The Hertz model assumes the contact between the AFM tip and the sample is elastic and without adhesion. In liquid environments, adhesion is very small or almost nonexistent because the liquid reduces any sticking forces. This makes the approach phase more suitable for using the Hertz model, as the measurements mainly reflect elastic deformation.

To calculate the elastic modulus, the JPK data processing software was used, following a systematic sequence of steps from the JPK data processing software manual (Figure 7.2) [87]. These operations were consistently applied across all analyzable force curves to ensure the reliability and reproducibility of the Young's modulus calculations. A detailed description of each step is provided below, with corresponding figures in Appendix A illustrating how each operation transforms the initial raw force curve. The settings used during each operation can also be seen, leading to the final step of fitting the data with the Hertz model to calculate the elastic modulus.

1. **Calibrate the cantilever**
   The first step in the process is calibrating the cantilever, which adjusts the sensitivity and spring constant parameters. These values were calculated just before the indentation measurements using the built-in contact-free method, which applies thermal noise analysis. The calibrated values were then stored in the force curve file and set as the default settings in the software. If no user-defined values are provided, the software applies default values of 25 nm/V for sensitivity and 50 nN/m for the spring constant.

   The nominal spring constant of the cantilever, as specified by the manufacturer, is 0.25 N/m. During the experiments, the calibrated spring constants ranged from 0.065 to 0.083 N/m, which falls within the manufacturer's specified range of 0.05 to 0.45 N/m. The sensitivity values ranged from 30 to 50 nm/V, consistent with the typical range of 30 to 100 nm/V. Since the measured values were within the expected ranges, no adjustments to the sensitivity or spring constant were necessary during data processing.

2. **Smoothing of force data**
   The second step involves applying a smoothing operation to the force data, which reduces high-frequency noise and produces a more refined curve essential for accurate curve fitting. This ensures that noise does not interfere with the precise determination of the elastic modulus.

   The smoothing operation uses mathematical algorithms to minimize fluctuations, often caused by thermal noise or other random variations. The software offers four smoothing methods: Gaussian, Boxcar, 2nd-order Savitzky-Golay, and 4th-order Savitzky-Golay, with the Gaussian method set as the default. This low-pass filtering technique replaces each data point with the weighted average of itself and its neighboring points within a defined range.

   The Gaussian method was found to effectively smooth the data while preserving the overall shape and key features of the force curve. For this reason, the smoothing method remained at the default setting.

3. **Baseline subtraction** The next step in the sequence is to eliminate any offset or tilt from the force curve. This is achieved through the baseline subtraction operation, which automatically calculates the average value of the curve in the baseline region. This region is located on the right side of the curve, far from the sample surface, and corresponds to when the AFM tip is approaching the sample. This baseline region should ideally be flat, where no force exists between the tip and the surface, providing the force baseline.

   Once the baseline is determined, it is subtracted from the entire force curve to correct for any offset or drift that may have occurred during measurement. This ensures that the force data used for the quantification of Young's modulus is accurate and reflects only the forces due to the interaction between the tip and the cell.

   In some cases, the flat region of the curve may not have an exact constant value. If there is a linear tilt in the baseline, it can be corrected during this operation by selecting the option "Offset + tilt." This option removes any linear drift in the baseline, ensuring that the force curve is properly aligned. By default, the extended curve is selected to adjust the baseline and set the zero-force level.

4. **Contact point determination**
   The next step in the data analysis is determining the contact point. The contact point operation automatically adjusts the x-offset by calculating the point where the force curve crosses the zero-force line and sets this as the zero of the x-axis. This adjustment is important because the focus is on the relative position of the force curve in relation to the sample surface, rather than the absolute position of the cantilever during the measurement. Accurate contact point determination is crucial for marking the start of the elastic region, as described by the Hertz model. It also ensures the correct calculation of indentation depth, which is essential for accurately determining the Young's modulus.

   The contact point determination operation identifies where the curve crosses the zero-force line, making it essential to perform baseline subtraction first. The previously applied smoothing operation further enhances contact point determination by ensuring that the first crossing of the smoothed curve through the zero-force line is more accurately identified. Together, these two operations improve the accuracy of the contact point determination.

5. **Calculate tip-sample separation**
   Operation 5, calculates the tip-sample separation, converting the force-distance curves into force-indentation curves. This operation corrects the measured heights for cantilever bending by calculating the indentation depth, which is the difference between the cantilever movement and the cantilever's vertical deflection. Already explained in subsection 3.2.1 of Part I.

   This is an important operation that must be applied before fitting the force curve with the Hertz model. The Hertz model is used to calculate the Young's modulus of the sample based on the indentation depth. Since the model assumes elastic deformation, it relies on an accurate indentation depth to determine the elastic properties. Without correcting for cantilever deflection, the indentation depth would be inaccurate, leading to incorrect results when fitting the curve with the Hertz model.

   After converting the force-distance curves into force-indentations curves, they are now ready to be fitted with the Hertz model to calculate the Young's modulus.

6. **Elasticity fit (Hertz model)**
   The final operation in the sequence involves extracting the Young's modulus (E) by fitting the experimental force-indentation curve to the theoretical Hertz model. This process requires specifying the geometry of the indenter, as each shape requires a specific fitting equation. While the cantilever used in this study has a hemispherical tip, a spherical tip shape is selected in the software for the analysis. This approximation is valid because, during small indentations, only the curved portion of the hemispherical tip contacts the cell, mimicking the behavior of a full sphere. The tip radius is set to 5 µm.

   The Hertz model for a spherical indenter is expressed by the equation [71]:

   $$F = \frac{4}{3} \cdot \frac{E}{1-\nu^2} \cdot R^{1/2} \cdot \delta^{3/2}$$

   In this equation, F represents the force applied to the sample, measured in newtons. Poisson's ratio, denoted by ν, is a dimensionless property of the material and is typically set to 0.5 for soft biological samples [71]. R refers to the radius of the spherical indenter, measured in meters, while δ represents the indentation depth into the sample, also in meters. Lastly, E denotes the Young's modulus of the sample, expressed in pascals, which is the parameter being determined.

   The fit is typically applied to the entire approach curve by default, however, the selection of the fitting range depends on both the sample characteristics and the quality of the baseline, more baseline data points generally improves accuracy.

   The Hertz model is valid only for small indentations, typically no more than 5–10$\%$ of the sample height. To meet this criterion, the fitting range is limited to 1 µm from the contact point onward. This ensures the maximum indentation depth is approximately 10$\%$ of the cell height, which is typically 6–10 µm. Limiting the depth to 1 µm also minimizes the influence of the substrate, such as the Petri dish, on the Young's modulus calculation.

   Once the parameters are set, the results, including the Young's modulus, contact point, and baseline, are displayed. Additionally, the residual root mean square (RMS) is provided, which quantifies the difference between the fitted curve and the force data, serving as an indicator of the fit's quality.

In summary, the process followed for analyzing the force-distance curves involved a series of operations to ensure accurate quantification of the Young's modulus. Both the cell-substrate and cell-cell force-distance curves were processed using the standard Hertz model with consistent parameters applied through the data processing software.

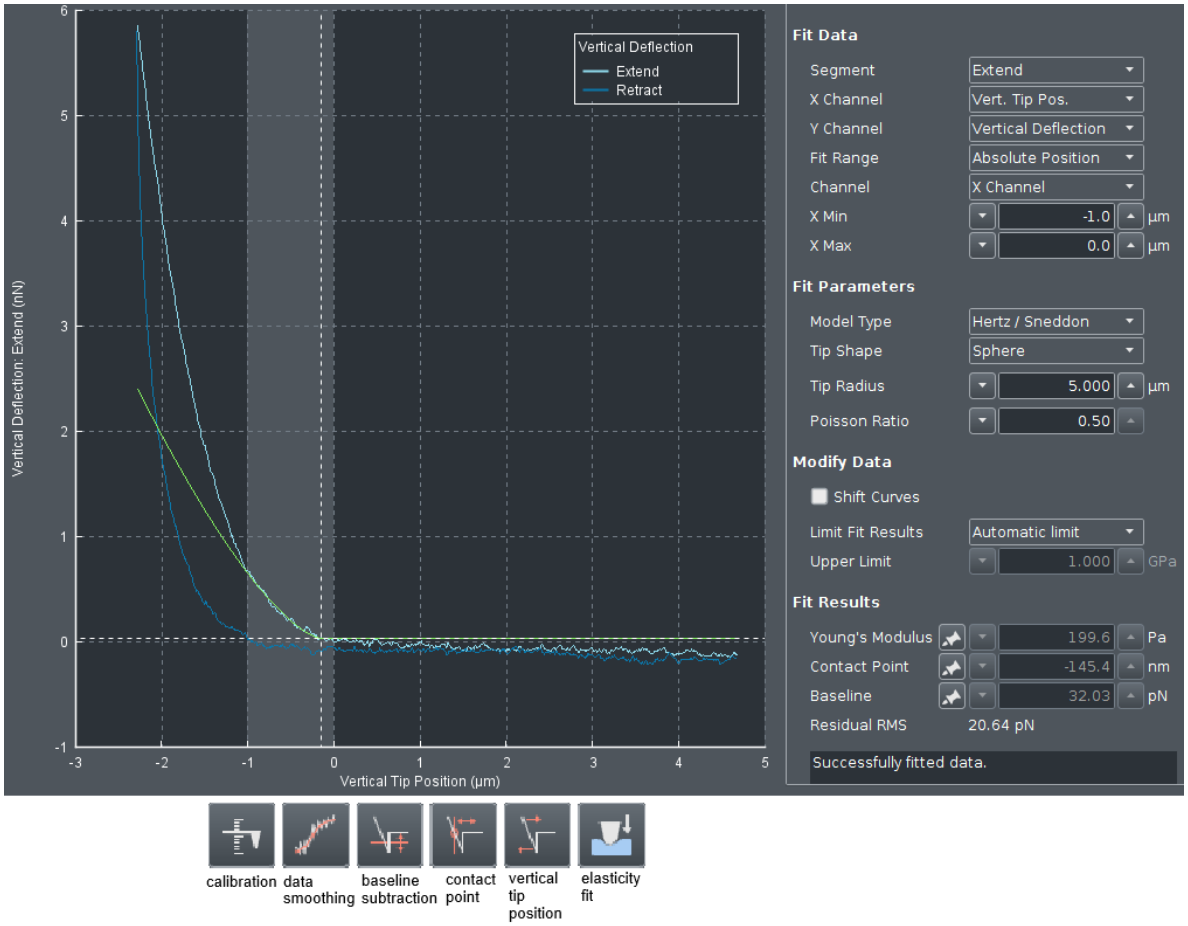

Figure 7.2: Representative force curve (cell-substrate configuration) with data analysis operations used to calculate the Young's modulus. Set the sensitivity and spring constant parameters based on the cantilever's calibration measurements. Smooth the force data, correct any offset or tilt in the baseline, and identify the contact point. Subtract the cantilever bending from the vertical cantilever movement to obtain the force-indentation curve. Finally, apply the Hertz model to calculate the Young's modulus. The Young's modulus of this curve, describing the elasticity of the cell surface, is about E = 199.6 Pa.

8

Results and discussion

This chapter presents the results obtained from the indentation measurements carried out on MCF-7 cells in two configurations, cell-substrate and cell-cell configurations. The Young's modulus for the cell-cell configuration is denoted as E_{cc}, while for the cell-substrate configuration, it is E_{cs}.

8.1. Validation of the AFM indentation method

The accuracy of the experimental method was validated using a material with a known elastic modulus. Polyacrylamide (PAM) hydrogel was chosen as the test material, and the method reliably quantified its Young's modulus, closely matching the manufacturer's specified value.

The same cantilever (SAA-SPH-5UM) with a hemispherical tip, used for cell measurements, was also employed for these tests. After calibration, the cantilever's spring constant was determined to be k = 0.078 N/m, and the sensitivity was measured as S = 36.44 nm/V. The hydrogel sample was indented with a setpoint force of 2 nN, an indentation speed of 1 µm/s, and a Z-length of 2 µm.

A total of 20 force curves were collected and analyzed. Data analysis was performed across the entire fitting range, as the force-indentation curve was accurately fitted, as shown in the appendix, where a hydrogel force curve is fitted using the Hertz model, sulting in an average elastic modulus of E_{hydrogel} = 24.08 ± 2.51 kPa, closely matching the manufacturer's value of 25 kPa.

This experiment confirmed the reliability and accuracy of the method, validating both the measurement and data analysis processes for subsequent cell-substrate and cell-cell measurements. However, these measurements will require consideration of additional factors when applied to cell-substrate and cell-cell interactions.

8.2. Young's modulus MCF-7 cell-substrate configuration

In the MCF-7 cell-substrate configuration, AFM indentation measurements were performed on a total of 2 Petri dishes and 4 cells (2 cells per dish). Figure 8.1 shows AFM images of Petri dish 2, cell A, right before the indentation measurements. The measurements were conducted using the following experimental parameters: setpoints of 4 and 6 nN, indentation speeds of 2 and 4 µm/s, and a Z-length of 10 µm. 5 analyzable force curves were collected from each of the 4 cell-substrate configurations, yielding a total of 20 force curves. These curves were analyzed using data processing operations from the JPK software, fitted to the Hertz model, to calculate the Young's modulus.

The results, based on Hertz contact model for a spherical indenter, are summarized in Table 8.1. The table presents the quantified Young's modulus (E) values for four MCF-7 cell-substrate configurations. A comparison of these values reveals significant differences both within the same Petri dish and across the two dishes:

1. **Petri dish 1**
    - Cell A has a higher Young's modulus (146.86 ± 20.11 Pa) compared to cell B (113.86 ± 12.13 Pa), indicating that cell A is more rigid than cell B in Petri dish 1.
    - The standard deviation for cell A (20.11 Pa) is higher than that for cell B (12.13 Pa), suggesting more variability in the measurements for cell A and notable variability even within the same dish.
2. **Petri dish 2**
    - Cell A in Petri dish 2 has a significantly higher Young's modulus (284.52 ± 51.72 Pa) compared to cell B (206.54 ± 56.57 Pa), indicating that cell A is much more rigid than cell B in Petri dish 2 , with a difference of 77.98 Pa.
    - The standard deviation for cell A (51.72 Pa) is slightly lower than that for cell B (56.57 Pa), suggesting slightly less variability in the measurements for cell A.
    - The standard deviation for both cells in Petri Dish 2 is larger than that in Petri Dish 1, indicating greater variability in measurements.
3. **Across dishes**
    - The average Young's modulus values for cells in Petri Dish 2 are significantly higher than those in Petri Dish 1. For instance, Cell A in Petri Dish 2 is nearly double the modulus of Cell A in Petri Dish 1, and Cell B in Petri Dish 2 is almost twice that of Cell B in Petri Dish 1. This indicates that cells in Petri dish 2 are generally more rigid and less elastic than those in Petri dish 1.
    - The standard deviations in Petri dish 2 are higher, indicating more variability in the measurements compared to Petri dish 1.

The overall mean elastic modulus for the cell-substrate configurations is E_{cs} = 187.95 ± 78.26 Pa, representing the average elasticity of the MCF-7 cells interacting with the substrate. The median is 160 Pa and the minimum value observed in the dataset was $E_{\text{cs,min}}$ = 100.7 Pa while the maximum value was $E_{\text{cs,max}}$ = 340.2 Pa.

Table 8.1: Average elastic modulus (± SD) of four MCF-7 cell-substrate configurations. The results are based on five force curves for each configuration.

	Young's Modulus [Pa]
Petri dish 1, cell A	$E_{\text{cs},1.}$ = 146.86 ± 20.11
Petri dish 1, cell B	$E_{\text{cs},2.}$ = 113.86 ± 12.13
Petri dish 2, cell A	$E_{\text{cs},3.}$ = 284.52 ± 51.72
Petri dish 2, cell B	$E_{\text{cs},4.}$ = 206.54 ± 56.57

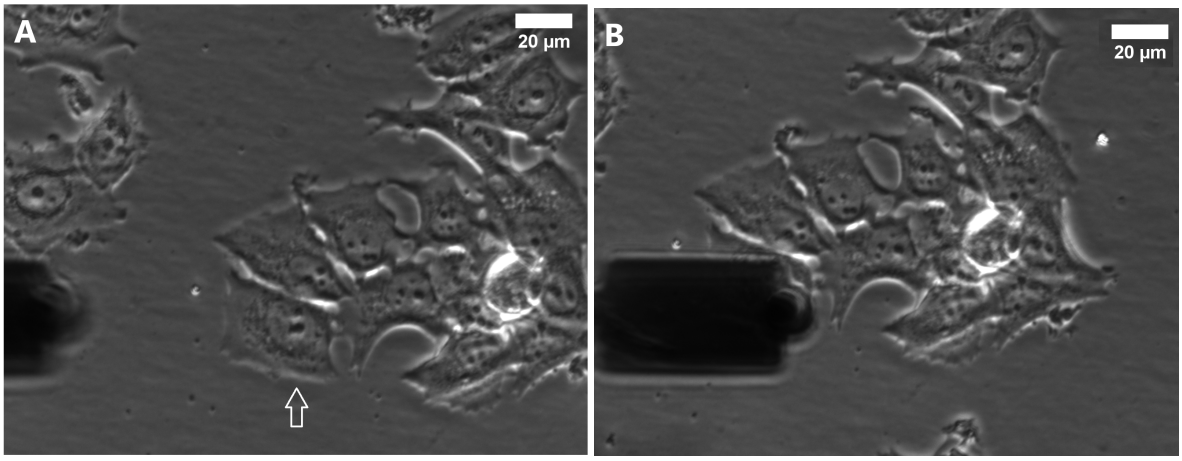

Figure 8.1: AFM images of the MCF-7 cell-substrate configuration (A) Close-up view of the selected cell in the cell-substrate configuration for AFM indentation, indicated by a white arrow. The black shadow (lower left) represents the cantilever before it approaches the cell. **(B)** View showing both the AFM cantilever and the cell, with the cantilever tip positioned directly above the cell-substrate configuration, now brought close to the cell surface, ready for indentation measurements.

8.3. Young's Modulus cell-cell configuration

In the MCF-7 cell-cell configuration, AFM indentation measurements were performed three petri dishes, with one cell measured from each dish. Figure 8.2 shows AFM images of Petri dish 2, cell A, captured prior to the indentation measurements.

The measurements were conducted using the following experimental parameters: setpoints of 6 and 8 nN, indentation speeds of 2 and 4 µm/s, and Z-length of 15 µm. From Petri dishes 1 and 2, five force curves each were collected, while from Petri dish 3 a total of 16 force curves were obtained, eight at a setpoint of 6 nN and eight at 8 nN. The other experimental parameters remained constant for petri dish 3. This resulted in a total of 26 force curves, which were analyzed using data processing operations from the JPK software to calculate the Young's modulus.

The results, based on the Hertz contact model for a spherical indenter, are summarized in Table 8.2. The table presents the quantified Young's modulus (E) values for four MCF-7 cell-cell configurations. A comparison of these values reveals significant differences both within the same Petri dish and across the three dishes:

1. **Petri dish 1 (Cell A):**
    - The Youngs Modulus $E_{\text{cc},1}$ = 278.98 ± 48.52 Pa is the highest among all measured configurations.
    - The relatively large standard deviation indicates significant variability in the measurements compared to other configurations.
2. Petri dish 2 (Cell B)
    - The Young's modulus $E_{\text{cc},2}$ = 158.14 ± 22.53 Pa is substantially lower than $E_{\text{cc},1}$, with a difference of 120.84 Pa, indicating that cell A in Petri dish 1 is much more rigid.
    - The smaller standard deviation implies more consistent measurements and possibly less variability in cell-cell interactions in this configuration.
3. **Petri dish 3**
    - Cell A ($E_{\text{cc},3}$ = 187.68 ± 21.07 Pa) and Cell B $E_{\text{cc},4}$ = 207.38 ± 20.64 Pa) exhibit closer values compared to other configurations.
    - The modulus of Cell B is higher than that of Cell A, with a difference of 19.70 Pa.
    - Both cells have relatively small standard deviations, indicating stable mechanical properties across measurements.
4. **Across configurations**
    - Highest ($E_{\text{cc},1}$) is nearly 1.8 times ($E_{\text{cc},2}$), showing significant differences in elasticity between configurations.

The overall mean elastic modulus for the cell-cell configuration, E_{cc} is determined to be 205.8 ± 50.88 Pa. This value represents the average elasticity of the MCF7-cells when interacting with other MCF-7 cells. The median value is 194.25 Pa and the minimum value $E_{\text{cc,min}}$ = 125.8 Pa and a maximum value $E_{\text{cc,max}}$ = 356.2 Pa.

Table 8.2: Average elastic modulus (± SD) of MCF-7 cell-cell configurations

	Young's Modulus [Pa]
Petri dish 1, cell A	$E_{\text{cc},1}$ = 278.98 ± 48.52
Petri dish 2, cell A	$E_{\text{cc},2}$ = 158.14 ± 22.53
Petri dish 3, cell A	$E_{\text{cc},3}$ = 187.68 ± 26.21
Petri dish 3, cell B	$E_{\text{cc},4}$ = 207.38 ± 20.64

To investigate the relationship between the degree of cell-cell contact and the elastic properties of MCF-7 cells, the following examines the percentage overlap of the top cell on the bottom cell in the four cell-cell configurations and compares it to the measured Young's modulus. The goal is to determine whether a higher percentage of overlap correlates with a higher or lower Young's modulus in cell-cell interactions.

As shown on Figure 8.2A, the top cell in the cell-cell configuration is not fully on top of the bottom cell. To better assess this, images of every cell-cell configurations were captured prior to the measurements, and the top and bottom cell areas were analyzed using ImageJ (Fiji) software. By calculating these areas, the percentage overlap of the top cell on the bottom cell was determined. In Table 8.3, the average elastic modulus (± SD) of MCF-7 cell-cell configurations is presented alongside the corresponding percentage overlap of the top cell on the bottom cell.

The data reveals variability in both the percentage overlap and the measured Young's modulus across the different Petri dish configurations. It can be observed that Petri dish 1, cell A shows a percentage overlap of 32.2$\%$ with a Young's modulus of 280.18 ± 48.48 Pa, which is the highest among the listed samples. However, despite this overlap, the Young's modulus for this configuration is notably higher than those of Petri dishes 2 and 3, suggesting that other factors may contribute to the variation in the elastic modulus. Petri dish 2, cell A exhibits a slightly higher percentage overlap at 33.7$\%$, yet its measured Young's modulus is significantly lower (158.14 ± 22.52 Pa) compared to Petri dish 1. Petri dish 3, cell A.1 and Petri dish 3, cell A.2 configurations both show a higher overlap percentage (42.8$\%$), but their Young's moduli are still lower than that of Petri dish 1, at 187.68 ± 21.07 Pa and 207.38 ± 20.64 Pa, respectively. These results suggest that while an increase in overlap percentage provides insight into the degree of cell-cell contact, the Young's modulus does not exhibit a straightforward correlation with overlap. In summary, while the percentage overlap provides useful insight into the degree of cell-cell contact, the variations in Young's modulus suggest that the relationship between overlap and elasticity is complex.

Table 8.3: Average elastic modulus (± SD) of MCF-7 cell-cell with percentage overlap

Percentage overlap $(\%)$ and Young's Modulus [Pa]		
Petri dish 1, cell A	32,20	$E_{cc,1}$ = 280.18 ± 48.48
Petri dish 2, cell A	33.70	$E_{cc,2}$ = 158.14 ± 22.52
Petri dish 3, cell A.1	42.80	$E_{cc,3}$ = 187.68 ± 21.07
Petri dish 3, cell A.2	42.80	$E_{cc,4}$ = 207.38 ± 20.64

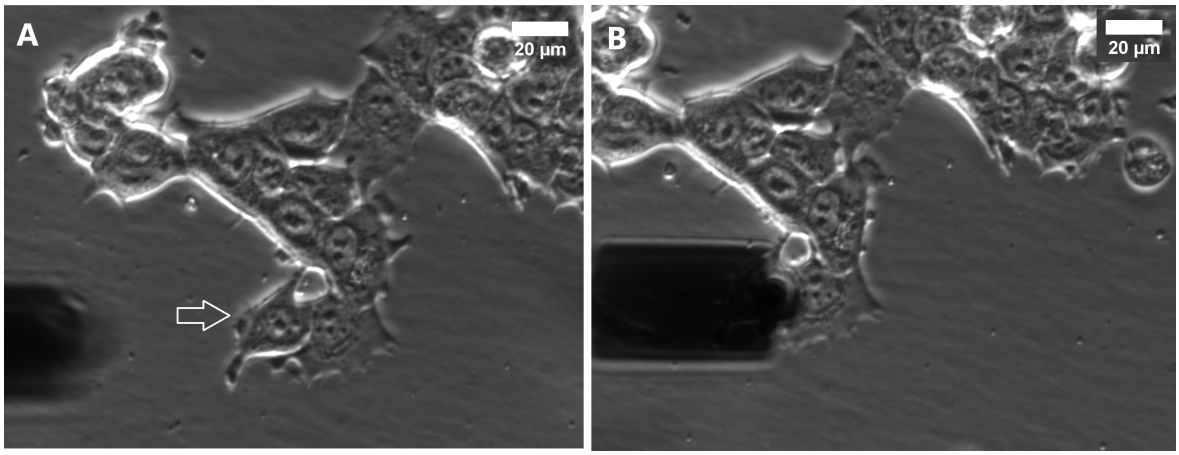

Figure 8.2: AFM images of the MCF-7 cell-cell configuration (A) Close-up view of the selected cell in cell-cell configuration for AFM indentation, indicated by a white arrow. The black shadow (lower left) represents the cantilever before it approaches the cell. **(B)** Focus on both the AFM cantilever and the cell, with the cantilever tip positioned directly above the cell-cell configuration, now brought close to the cell surface, ready to perform indentation measurements on the top of the cell.

8.4. Comparison between the cell-substrate and cell-cell results

The comparison of Young's modulus values for the MCF-7 cell-substrate and cell-cell configurations reveals significant differences in the elastic properties of the cells under different conditions. The data is visualized using a boxplot, as shown in Figure 8.3. This boxplot highlights these differences, illustrating variations in both the median values and the spread of the data. The key observations from the boxplot:

1. **Cell-substrate configuration**
    - Range: The values range from 100.7 Pa to 340.2 Pa. This shows a broad spread, indicating considerable variability in the mechanical properties of the cells when attached to the substrate.
    - Median: The median value is approximately 159 Pa, suggesting that half of the values are below this point, and half are above.
    - The average value is around 187.95 ± 78.26 Pa, which indicates a relatively higher mean compared to the median due to the presence of some higher outliers, such as the 340.2 Pa value.
2. **Cell-cell configuration**
    (a) Range: The values range from 125.8 Pa to 356.2 Pa. While the maximum value is similar to the cell-substrate configuration, the minimum value is higher than that of the cell-substrate configuration.
    (b) Median: The median is 195.2 Pa, which is higher than the cell-substrate median, indicating that a larger proportion of the data points in the cell-cell configuration are associated with stiffer mechanical properties.
    (c) Mean: The mean value is around 205.8 ± 50.88 Pa, which is significantly higher than the cell-substrate mean, reflecting the overall lower elasticity in the cell-cell configuration.

    Comparison of elastic modulus
    (a) Overall elasticity: On average, cells in the cell-cell configuration show higher Young's Modulus than those in the cell-substrate configuration. The mean Young's modulus for the cell-cell configuration is approximately 205.8 ± 50.88 Pa, while the mean for the cell-substrate configuration is about 187.95 ± 78.26 Pa. This suggests that the elastic properties of MCF-7 cells are generally less elastic when interacting with other cells.
    (b) Median values: The median Young's modulus for the cell-cell configuration is 195.2 Pa, which is noticeably higher than the 159 Pa median for the cell-substrate configuration. This indicates that a larger portion of the cell-cell values lie in the higher elastic modulus range, suggesting that most cells in this configuration experience stronger intercellular forces compared to their adhesion to the substrate.
3. **Distribution and Spread:** Both configurations show a wide range of values, with the cell-substrate configuration exhibiting more variability (as reflected in the higher standard deviation). The broader spread in the cell-substrate configuration indicates that the mechanical properties of cells in this configuration are more heterogeneous. The cell-cell configuration, while also exhibiting variability, shows a more consistent elasticity profile with a lower standard deviation, suggesting that the intercellular interactions lead to more uniform mechanical properties among the cells. This suggests that the intercellular interactions promote more uniform mechanical properties, with less fluctuation compared to the cell-substrate configuration.
4. **Outliers:** In the cell-cell configuration the value of 356.2 Pa appears as a outlier.

In summary, the analysis reveals that MCF-7 cells exhibit a higher elastic modulus in the cell-cell configuration compared to the cell-substrate configuration. Overall, the obtained Young's modulus values are lower than those reported in the literature. These differences are likely attributed to a combination of biological heterogeneity among cells and variations in experimental conditions, which are further discussed in the following section.

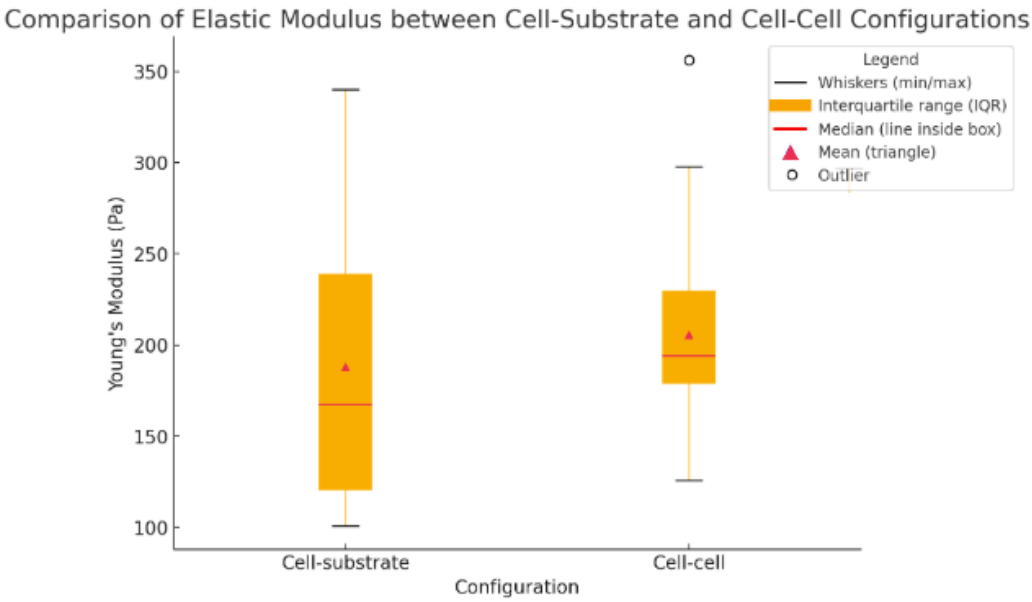

Figure 8.3: Boxplots of quantified Young's modulus E (Pa) Comparison of experimental results for MCF-7 cells in cell-substrate and cell-cell configurations. The boxes in the boxplot represent the interquartile range (IQR), which contains the middle 50% of the data. This range is bounded by the 25th percentile (Q1) at the lower edge of the box and the 75th percentile (Q3) at the upper edge. The box indicates where most of the data is concentrated. The whiskers extend from the edges of the box, representing the range of the data excluding outliers. Data points beyond this range are considered outliers. The circle marker ('o') at the cell-cell configuration represents an outlier, which is a data point that lies outside the whiskers. The mean value is indicated by a triangle, and the median value is represented by a horizontal line inside the box.

8.5. Discussion

1. **Variability in Young's modulus results**
   The overall lower values for Young's modulus observed in this study, compared to those reported in the literature, are likely due to a combination of biological heterogeneity among cells and differences in experimental methodology. AFM measurements are sensitive to factors such as probe geometry, indentation depth, and sample preparation, all of which can contribute to significant variations in the measured elasticity.

2. **Lack of standardization in experimental protocols and analysis methods**
   The lack of standardization in experimental protocols and analysis methods contributes to the difficulty in reproducing precise quantitative values across studies. As a result, elasticity measurements obtained via AFM measurements are often discussed qualitatively rather than quantitatively due to these variations. The lack of standardization in experimental protocols and analysis methods contributes to the difficulty in reproducing precise quantitative values across studies. Thus, discrepancies in reported elastic moduli, including the lower values observed in this study, are not uncommon in AFM-based research.

3. **Limitations of the Hertz model**
   The Hertz model, which assumes a perfectly elastic, homogeneous, and isotropic material, has limitations when applied to biological samples such as cells. Cells are viscoelastic and exhibit behaviors that deviate from these assumptions, making the Hertz model an imperfect fit. Despite these limitations, the Hertz model remains the most widely used model for characterizing the elastic properties of cells, even though alternative models have been proposed to address some of its shortcomings. This highlights the need for the scientific community to use simplified or approximate methods when studying biological systems. These approximations are necessary because existing theoretical models don't completely match or account for the complex conditions found in real-life experiments, especially when applied to biological samples such as cells.

4. **Experimental method** Part of the variation in reported Young's modulus values arises from differences in controllable experimental factors, such as cantilever tip geometry, temperature, indentation speed, storage medium, cell condition, and the specific experimental method. These experimental variations make direct comparison of results between studies challenging. Therefore, it is crucial to standardize experimental protocols and clearly report the conditions under which measurements are taken. This would enable more consistent results and better comparability across studies, leading to a more comprehensive understanding of the elastic properties of biological tissues.

5. **Experimental parameters**
   Clearly stating all experimental parameters is crucial when measuring elasticity, as these factors directly influence the results. However, many published studies fail to provide these essential details. For example, in AFM indentation experiments, critical information such as the indentation speed of the cantilever is often not included. Without these specifics, comparing results across different research groups becomes challenging, which can undermine the reliability of the findings. Accurate measurements, therefore, require careful control and consistent reporting of experimental parameters.

6. **Insufficient Data for Comprehensive Elasticity Analysis**
   To accurately describe a sample's elastic properties, it is essential to record and evaluate a large number of force-distance curves. Once the AFM is properly set up, it can be programmed to automatically collect these indentation curves using various experimental parameters, such as setpoint force, indentation speed, and position across the sample. Additionally, the data analysis process can be automated, enabling efficient and consistent evaluation of the mechanical properties across multiple regions of the sample. However, due to limitations in the data collection process, a larger dataset would be required to fully capture the variability and characterize the sample's elasticity with greater accuracy. This would ensure a more robust analysis and minimize potential biases or gaps in the results. Given the variability observed in the current dataset, acquiring additional data points would improve the reliability of the results and reduce the im-

pact of outliers. A more comprehensive dataset would provide a clearer and more consistent characterization of the sample's elasticity.

9 Conclusion

In conclusion, the elastic modulus of the MCF-7 human breast cancer cell line was determined through AFM force spectroscopy indentation experiments using a micro-sized cantilever with hemispherical tip. The findings reveal that the Young's modulus for the cell-substrate configuration was E_{cs} = 187.95 ± 40.08 Pa, while for the cell-cell configuration, it was E_{cc} = 205.8 ± 50.88 Pa. Although a difference was anticipated, the results show only a slight variation between the two configurations. The values obtained in this study exhibit considerable variability, likely due to the inherent heterogeneity of the cells and differences in experimental conditions. This variability emphasized the importance of ensuring repeatability and reliability in experimental setups while carefully controlling experimental parameters. Moreover, these elastic modulus values should primarily be interpreted as relative, providing comparative insights within the same experimental procedure rather than as absolute material properties, due to limitations in data processing and inherent complexities in the measurements.

Bibliography

[1] Denis Wirtz, Konstantinos Konstantopoulos, and Peter C. Searson. The physics of cancer: The role of physical interactions and mechanical forces in metastasis. *Nature Reviews Cancer*, 11:512–522, 7 2011.

[2] Klaus Pantel and Ruud H Brakenhoff. Dissecting the metastatic cascade. *Nature reviews cancer*, 4(6):448–456, 2004.

[3] Volha Liaudanskaya, Disha Sood, and David L. Kaplan. *Chapter 24 - Mechanical Determinants of Tissue Development*. Academic Press, Boston, third edition edition, 2019.

[4] Sarah E Cross, Yu-Sheng Jin, Jianyu Rao, and James K Gimzewski. Nanomechanical analysis of cells from cancer patients. *Nature nanotechnology*, 2(12):780–783, 2007.

[5] Wenwei Xu, Roman Mezencev, Byungkyu Kim, Lijuan Wang, John McDonald, and Todd Sulchek. Cell stiffness is a biomarker of the metastatic potential of ovarian cancer cells. 2012.

[6] Q. S. Li, G. Y.H. Lee, C. N. Ong, and C. T. Lim. Afm indentation study of breast cancer cells. *Biochemical and Biophysical Research Communications*, 374:609–613, 10 2008.

[7] Małgorzata Lekka, Katarzyna Pogoda, Justyna Gostek, Olesya Klymenko, Szymon Prauzner-Bechcicki, Joanna Wiltowska-Zuber, Justyna Jaczewska, Janusz Lekki, and Zbigniew Stachura. Cancer cell recognition–mechanical phenotype. *Micron*, 43(12):1259–1266, 2012.

[8] G. Binnig, C. F. Quate, and Ch. Gerber. Atomic force microscope. *Phys. Rev. Lett.*, 56:930–933, Mar 1986.

[9] Yves F Dufrêne, Toshio Ando, Ricardo Garcia, David Alsteens, David Martinez-Martin, Andreas Engel, Christoph Gerber, and Daniel J Müller. Imaging modes of atomic force microscopy for application in molecular and cell biology. *Nature nanotechnology*, 12(4):295–307, 2017.

[10] Michael Krieg, Gotthold Fläschner, David Alsteens, Benjamin M. Gaub, Wouter H. Roos, Gijs J.L. Wuite, Hermann E. Gaub, Christoph Gerber, Yves F. Dufrêne, and Daniel J. Müller. Atomic force microscopy-based mechanobiology. *Nature Reviews Physics*, 1:41–57, 1 2019.

[11] Subra Suresh. Biomechanics and biophysics of cancer cells. *Acta Biomaterialia*, 3:413–438, 2007.

[12] Eldra Pearl Solomon. *Introduction to human anatomy and physiology*. Elsevier Health Sciences, 2015.

[13] url = https://www.cancer.gov/publications/dictionaries/cancer-terms/def/cell year = 2000 National Cancer Institute (NIH), title = NCI Dictionary of Cancer Terms.

[14] Anne R Haake and Renata R Polakowska. Cell death by apoptosis in epidermal biology. *Journal of Investigative Dermatology*, 101(2):107–112, 1993.

[15] Scientific American. Editors. *The Science of Cancer*. Rosen Publishing Group, 2022.

[16] Keith R Loeb and Lawrence A Loeb. Significance of multiple mutations in cancer. *Carcinogenesis*, 21(3):379–385, 2000.

[17] Marikki Laiho and Leena Latonen. Cell cycle control, dna damage checkpoints and cancer. *Annals of medicine*, 35(6):391–397, 2003.

[18] Helen K Matthews, Cosetta Bertoli, and Robertus AM de Bruin. Cell cycle control in cancer. *Nature Reviews Molecular Cell Biology*, 23(1):74–88, 2022.

[19] Mark AJ Chaplain and G Lolas. Mathematical modelling of cancer invasion of tissue: dynamic heterogeneity. *Networks Heterog. Media*, 1(3):399–439, 2006.

[20] url = https://www.genome.gov/genetics-glossary/Cancer National human genome research institute, title = Cancer.

[21] Jun Qin, Xinpu Chen, Xin Xie, Ming-Jer Tsai, and Sophia Tsai. Coup-tfii regulates tumor growth and metastasis by modulating tumor angiogenesis. *Proceedings of the National Academy of Sciences of the United States of America*, 107:3687–92, 02 2010.

[22] Serena PH Chiang, Ramon M Cabrera, and Jeffrey E Segall. Tumor cell intravasation. *American Journal of Physiology-Cell Physiology*, 311(1):C1–C14, 2016.

[23] Patrizia Paterlini-Brechot and Naoual Linda Benali. Circulating tumor cells (ctc) detection: clinical impact and future directions. *Cancer letters*, 253(2):180–204, 2007.

[24] R Riahi, YL Yang, H Kim, L Jiang, PK Wong, and Y Zohar. A microfluidic model for organ-specific extravasation of circulating tumor cells. *Biomicrofluidics*, 8(2), 2014.

[25] Nicolas Reymond, Bárbara Borda d'Água, and Anne J Ridley. Crossing the endothelial barrier during metastasis. *Nature Reviews Cancer*, 13(12):858–870, 2013.

[26] Gregg L Semenza. The hypoxic tumor microenvironment: A driving force for breast cancer progression. *Biochimica et Biophysica Acta (BBA)-Molecular Cell Research*, 1863(3):382–391, 2016.

[27] Fabian Spill, Daniel S Reynolds, Roger D Kamm, and Muhammad H Zaman. physical microenvironment on tumor progression and metastasis. *Current opinion in biotechnology*, 40:41–48, 2016.

[28] Nicole M. Anderson and M. Celeste Simon. The tumor microenvironment. *Current Biology*, 30:R921–R925, 8 2020.

[29] Xiaoqi Mao, Jin Xu, Wei Wang, Chen Liang, Jie Hua, Jiang Liu, Bo Zhang, Qingcai Meng, Xianjun Yu, and Si Shi. Crosstalk between cancer-associated fibroblasts and immune cells in the tumor microenvironment: new findings and future perspectives. *Molecular cancer*, 20(1):1–30, 2021.

[30] Frances R Balkwill, Melania Capasso, and Thorsten Hagemann. The tumor microenvironment at a glance. *Journal of cell science*, 125(23):5591–5596, 2012.

[31] Douglas Hanahan and Lisa M Coussens. Accessories to the crime: functions of cells recruited to the tumor microenvironment. *Cancer cell*, 21(3):309–322, 2012.

[32] Marta Truffi, Luca Sorrentino, and Fabio Corsi. *Fibroblasts in the Tumor Microenvironment*, volume 1234. Springer, 2020.

[33] American association for cancer research. How the tumor microenvironment supports or stifles cancer growth.

[34] Role of the tumor microenvironment in tumor progression and the clinical applications (review). *Oncology Reports*, 35:2499–2515, 5 2016.

[35] Vanessa Barriga, Nyanbol Kuol, Kulmira Nurgali, and Vasso Apostolopoulos. The complex interaction between the tumor micro-environment and immune checkpoints in breast cancer. *Cancers*, 11, 8 2019.

[36] Isabella Ellinger and Adolf Ellinger. Smallest unit of life: cell biology. *Comparative medicine: Anatomy and physiology*, pages 19–33, 2014.

[37] M Tartibi and K Komvopoulos. *Characterization of the Mechanical Behavior of Cell Components with an Atomic Force Microscope*, volume 44199. 2010.

[38] William Martin. Archaebacteria (archaea) and the origin of the eukaryotic nucleus. *Current opinion in microbiology*, 8(6):630–637, 2005.

[39] Emad Moeendarbary and Andrew R Harris. Cell mechanics: principles, practices, and prospects. *Wiley Interdisciplinary Reviews: Systems Biology and Medicine*, 6(5):371–388, 2014.

[40] Yusuf S Khan and Aisha Farhana. Histology, cell. 2020.

[41] Othmène Benazieb. *Rheology of lipids layers at molecular length scales*. PhD thesis, Université de Strasbourg, 2020.

[42] Haibo Huang, Cihai Dai, Hao Shen, Mingwei Gu, Yangjun Wang, Jizhu Liu, Liguo Chen, and Lining Sun. Recent advances on the model, measurement technique, and application of single cell mechanics. *International Journal of Molecular Sciences*, 21(17):6248, 2020.

[43] Lin Bo and Richard E Waugh. Determination of bilayer membrane bending stiffness by tether formation from giant, thin-walled vesicles. *Biophysical journal*, 55(3):509–517, 1989.

[44] Virginia A Shepherd. The cytomatrix as a cooperative system of macromolecular and water networks. *Current topics in developmental biology*, 75:171–223, 2006.

[45] Jan Lammerding. Mechanics of the nucleus. *Comprehensive physiology*, 1(2):783, 2011.

[46] Cell mechanics and the cytoskeleton. *Nature*, 463:485–492, 1 2010.

[47] Kristina Haase and Andrew E Pelling. Investigating cell mechanics with atomic force microscopy. *Journal of The Royal Society Interface*, 12(104):20140970, 2015.

[48] Gawain Thomas, Nancy A Burnham, Terri Anne Camesano, and Qi Wen. Measuring the mechanical properties of living cells using atomic force microscopy. *JoVE (Journal of Visualized Experiments)*, (76):e50497, 2013.

[49] Revital Kristal-Muscal, Liron Dvir, Ma'Ayan Schvartzer, and Daphne Weihs. Mechanical interaction of metastatic cancer cells with a soft gel. *Procedia IUTAM*, 12:211–219, 2015.

[50] Manfred Radmacher. Studying the mechanics of cellular processes by atomic force microscopy. 83:347–372, 2007.

[51] S Kasas, X Wang, H Hirling, R Marsault, B Huni, A Yersin, R Regazzi, G Grenningloh, B Riederer, L Forro, et al. Superficial and deep changes of cellular mechanical properties following cytoskeleton disassembly. *Cell motility and the cytoskeleton*, 62(2):124–132, 2005.

[52] Martha E Grady, Russell J Composto, and David M Eckmann. Cell elasticity with altered cytoskeletal architectures across multiple cell types. *Journal of the mechanical behavior of biomedical materials*, 61:197–207, 2016.

[53] Thomas D. Pollard and John A. Cooper. Actin, a central player in cell shape and movement. *Science*, 326:1208–1212, 11 2009.

[54] Jay Shankar and Ivan R Nabi. Actin cytoskeleton regulation of epithelial mesenchymal transition in metastatic cancer cells. *PloS one*, 10(3):e0119954, 2015.

[55] Intracellular mechanics and activity of breast cancer cells correlate with metastatic potential. *Cell Biochemistry and Biophysics*, 63:199–209, 7 2012.

[56] Alexander X Cartagena-Rivera, Jeremy S Logue, Clare M Waterman, and Richard S Chadwick. Actomyosin cortical mechanical properties in nonadherent cells determined by atomic force microscopy. *Biophysical journal*, 110(11):2528–2539, 2016.

[57] Valérie M Laurent, Redouane Fodil, Patrick Cañadas, Sophie Féréol, Bruno Louis, Emmanuelle Planus, and Daniel Isabey. Partitioning of cortical and deep cytoskeleton responses from transient magnetic bead twisting. *Annals of biomedical engineering*, 31:1263–1278, 2003.

[58] Marita L Rodriguez, Patrick J McGarry, and Nathan J Sniadecki. Review on cell mechanics: experimental and modeling approaches. *Applied Mechanics Reviews*, 65(6):060801, 2013.

[59] Eimear B. Dolan, Stefaan W. Verbruggen, and Rebecca A. Rolfe. *Techniques for studying mechanobiology*. Elsevier, 1 2018.

[60] Charlotte Alibert, Bruno Goud, and Jean-Baptiste Manneville. Are cancer cells really softer than normal cells? *Biology of the Cell*, 109, 02 2017.

[61] Hiroaki Ito and Makoto Kaneko. On-chip cell manipulation and applications to deformability measurements. *ROBOMECH journal*, 7(1):3, 2020.

[62] Ashwini Shinde, Kavitha Illath, Pallavi Gupta, Pallavi Shinde, Ki Taek Lim, Moeto Nagai, and Tuhin Subhra Santra. A review of single□cell adhesion force kinetics and applications. *Cells*, 10:1–46, 3 2021.

[63] A comparison of methods to assess cell mechanical properties. *Nature Methods*, 15:491–498, 6 2018.

[64] Dimitrios Kirmizis and Stergios Logothetidis. Atomic force microscopy probing in the measurement of cell mechanics. *International journal of nanomedicine*, pages 137–145, 2010.

[65] Daniel J Müller and Yves F Dufrene. Atomic force microscopy as a multifunctional molecular toolbox in nanobiotechnology. *Nature nanotechnology*, 3(5):261–269, 2008.

[66] Xinlong Wang, Yingjun Yang, Xiaohong Hu, Naoki Kawazoe, Yingnan Yang, and Guoping Chen. Morphological and mechanical properties of osteosarcoma microenvironment cells explored by atomic force microscopy. *Analytical sciences*, 32(11):1177–1182, 2016.

[67] Małgorzata Lekka. Discrimination between normal and cancerous cells using afm. *Bionanoscience*, 6:65–80, 2016.

[68] Judit Kámán, Róbert Huszánk, and Attila Bonyár. Towards more reliable afm force-curve evaluation: a method for spring constant selection, adaptive lever sensitivity calibration and fitting boundary identification. *Micron*, 125:102717, 2019.

[69] Sergey Belikov, John Alexander, Craig Wall, Ivan Yermolenko, Sergei Magonov, and Ivan Malovichko. Thermal tune method for afm oscillatory resonant imaging in air and liquid. In *2014 American Control Conference*, pages 1009–1014. IEEE, 2014.

[70] JPK$_{I}nstruments_{A}G.Nanowizardafmusermanualversion6.0.[Accessed01-12-2024]$.

[71] JPK Application Note. Determining the elastic modulus of biological samples using the atomic force microscope. *JPK Instruments [cit. 2022-04-27]. Dostupné z: https://www. jpk. com/app-technotes-img/AFM/pdf/jpk-app-elastic-modulus*, pages 14–1.

[72] Malgorzata Kopycinska-Müller, Roy H Geiss, and Donna C Hurley. Contact mechanics and tip shape in afm-based nanomechanical measurements. *Ultramicroscopy*, 106(6):466–474, 2006.

[73] Force-Distance Spectroscopy — parksystems.com. `https://www.parksystems.com/park-spm-modes/95-force-measurement/244-force-distance-spectroscopy`. [Accessed 21-11-2023].

[74] Heinrich Hertz. Über die berührung fester elastischer körper. *J reine und angewandte Mathematik*, 92:156, 1881.

[75] Ian N Sneddon. The relation between load and penetration in the axisymmetric boussinesq problem for a punch of arbitrary profile. *International journal of engineering science*, 3(1):47–57, 1965.

[76] Kenneth Langstreth Johnson, Kevin Kendall, and aAD Roberts. Surface energy and the contact of elastic solids. *Proceedings of the royal society of London. A. mathematical and physical sciences*, 324(1558):301–313, 1971.

[77] Clayton T McKee, Julie A Last, Paul Russell, and Christopher J Murphy. Indentation versus tensile measurements of young's modulus for soft biological tissues. *Tissue Engineering Part B: Reviews*, 17(3):155–164, 2011.

[78] Malgorzata Lekka, Piotr Laidler, Dorota Gil, Janusz Lekki, Zbigniew Stachura, and AZ Hrynkiewicz. Elasticity of normal and cancerous human bladder cells studied by scanning force microscopy. *European Biophysics Journal*, 28:312–316, 1999.

[79] Sangwoo Kwon, Woochul Yang, Donggerami Moon, and Kyung Kim. Comparison of cancer cell elasticity by cell type. *Journal of Cancer*, 11:5403–5412, 07 2020.

[80] Jorge R Ramos, Joanna Pabijan, Ricardo Garcia, and Malgorzata Lekka. The softening of human bladder cancer cells happens at an early stage of the malignancy process. *Beilstein journal of nanotechnology*, 5(1):447–457, 2014.

[81] Elsa Correia Faria, Nan Ma, Ehsan Gazi, Peter Gardner, Mick Brown, Noel W Clarke, and Richard D Snook. Measurement of elastic properties of prostate cancer cells using afm. *Analyst*, 133(11):1498–1500, 2008.

[82] Yu M Efremov, AA Dokrunova, AV Efremenko, MP Kirpichnikov, KV Shaitan, and OS Sokolova. Distinct impact of targeted actin cytoskeleton reorganization on mechanical properties of normal and malignant cells. *Biochimica et Biophysica Acta (BBA)-Molecular Cell Research*, 1853(11):3117–3125, 2015.

[83] Eva Potthoff, Orane Guillaume-Gentil, Dario Ossola, Jerome Polesel, Salomé LeibundGut-Landmann, Tomaso Zambelli, and Julia Vorholt. Rapid and serial quantification of adhesion forces of yeast and mammalian cells. *PloS one*, 7:e52712, 12 2012.

[84] Juan Carlos Gil-Redondo, Andreas Weber, Barbara Zbiral, José L Toca-Herrera, et al. Substrate stiffness modulates the viscoelastic properties of mcf-7 cells. *Journal of the Mechanical Behavior of Biomedical Materials*, 125:104979, 2022.

[85] Moharram Habibnejad Korayem, YH Sooha, and Z Rastegar. Mcf-7 cancer cell apparent properties and viscoelastic characteristics measurement using afm. *Journal of the Brazilian Society of Mechanical Sciences and Engineering*, 40:1–11, 2018.

[86] Matrigen. Matrigen petrisoft 35 hydrogel bound to a 35 mm polystyrene dish.

[87] Bruker-JPK Instruments, Germany. Atomic force microscope nanowizard v bioscience.

[88] Bruker-JPK Instruments, Germany.

[89] Surya Bansi Singh, Shatruhan Singh Rajput, Shivprasad Patil, and Deepa Subramanyam. Protocol for measuring mechanical properties of live cells using atomic force microscopy. *STAR protocols*, 5(1):102870, 2024.

III
Appendix

A

Figures data analysis operations

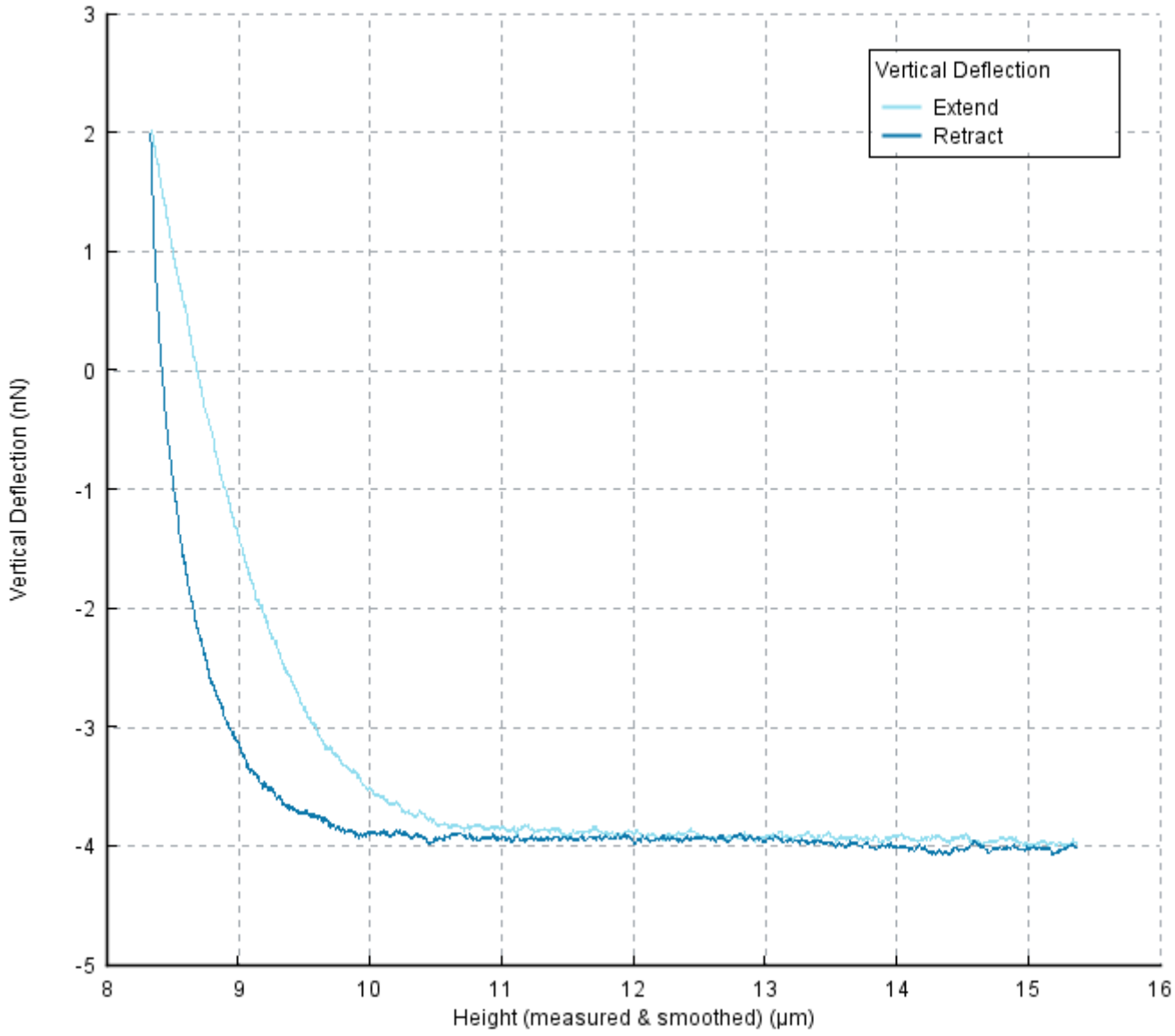

Figure A.1: Calibrate the cantilever

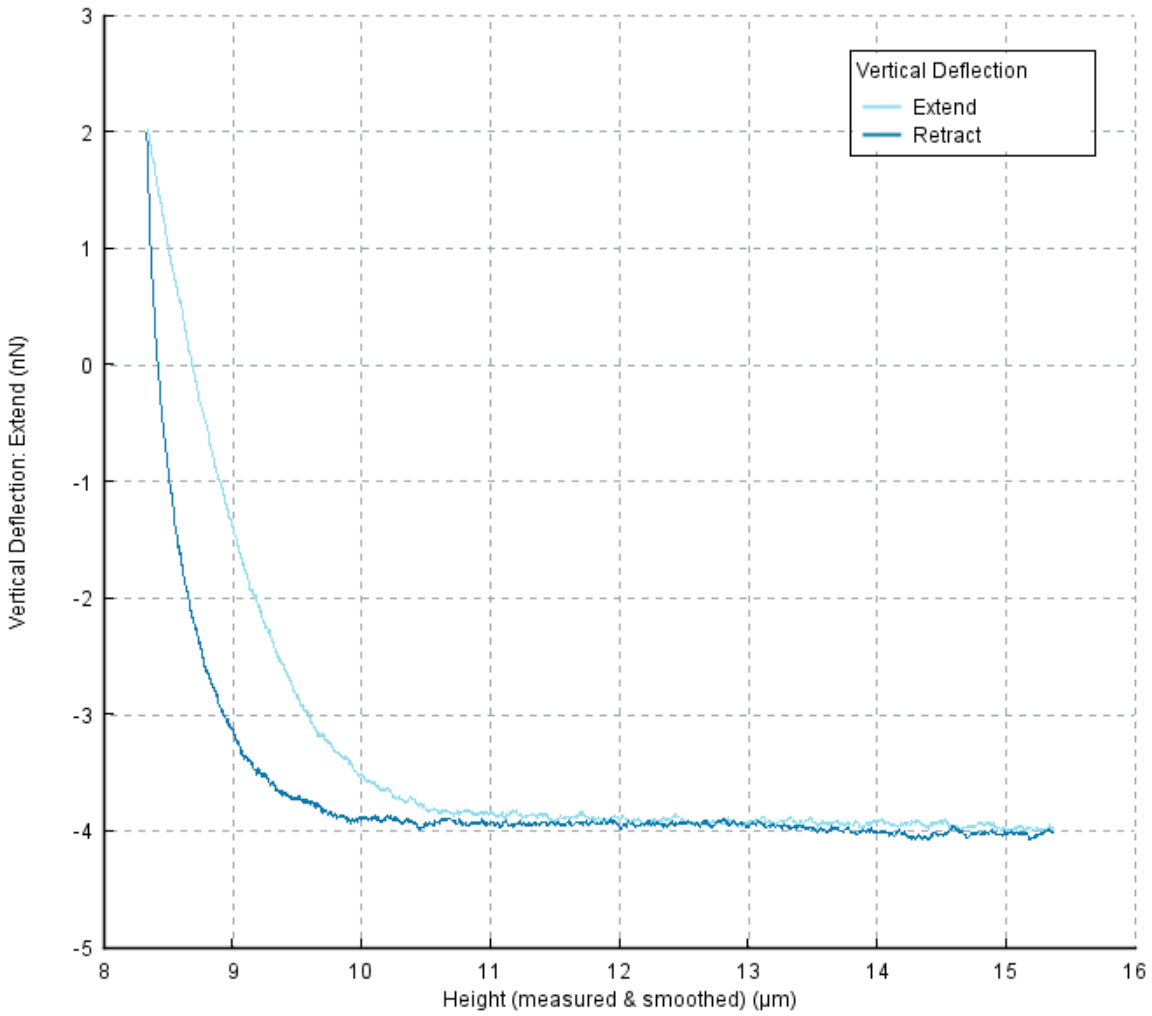

Figure A.2: Smooth the Force Data

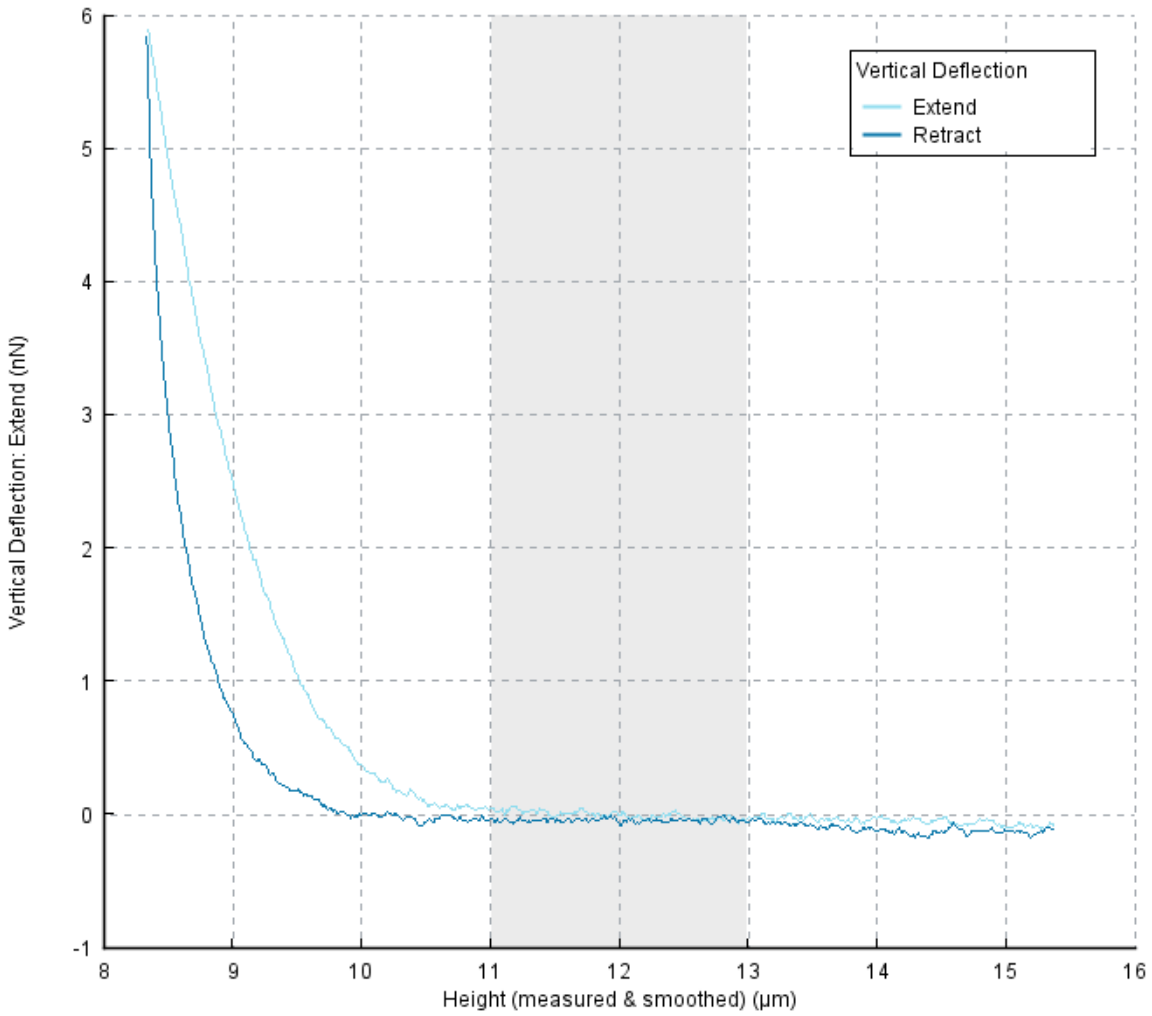

Figure A.3: Adjust the Baseline to set the zero force level

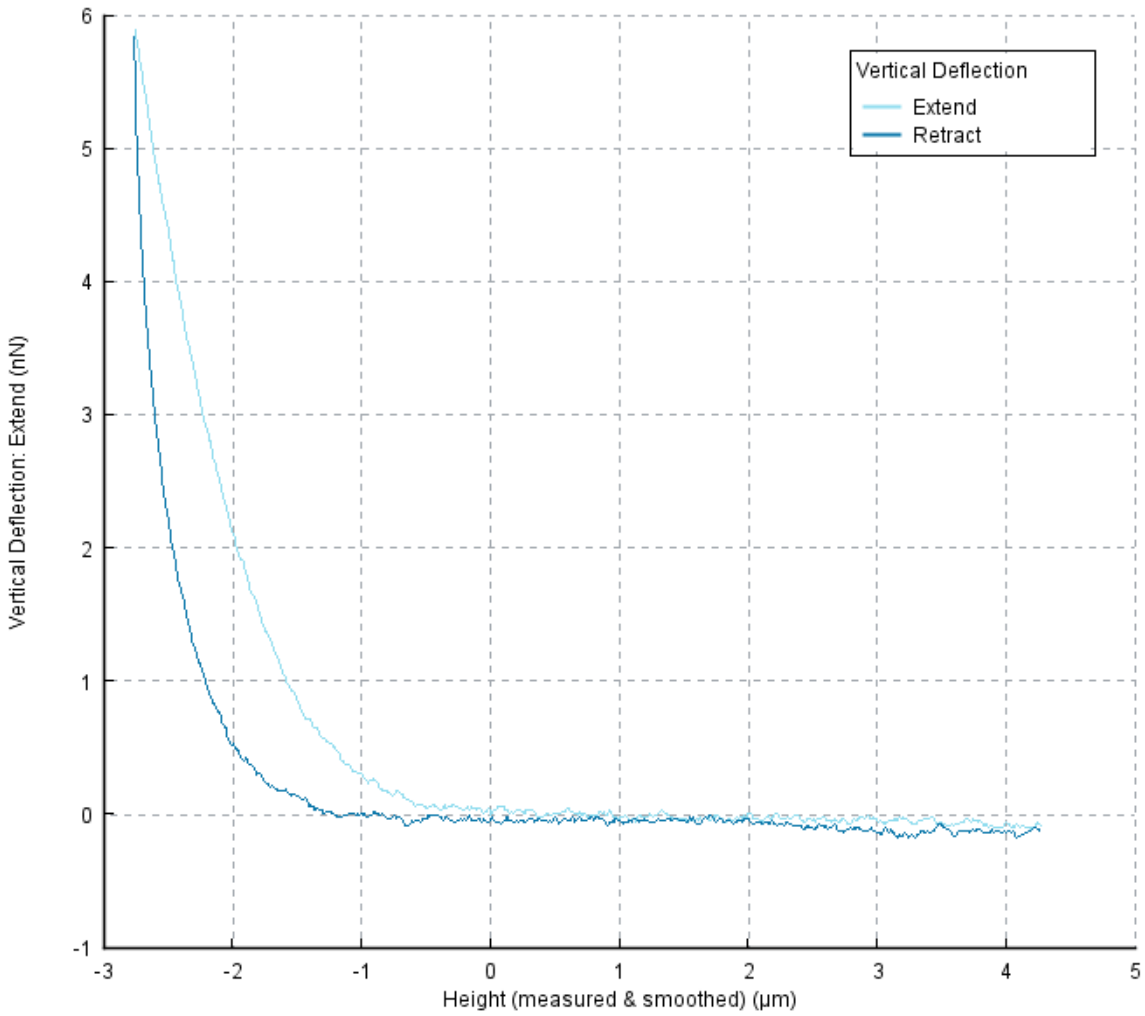

Figure A.4: Find the Contact Point of the Curve

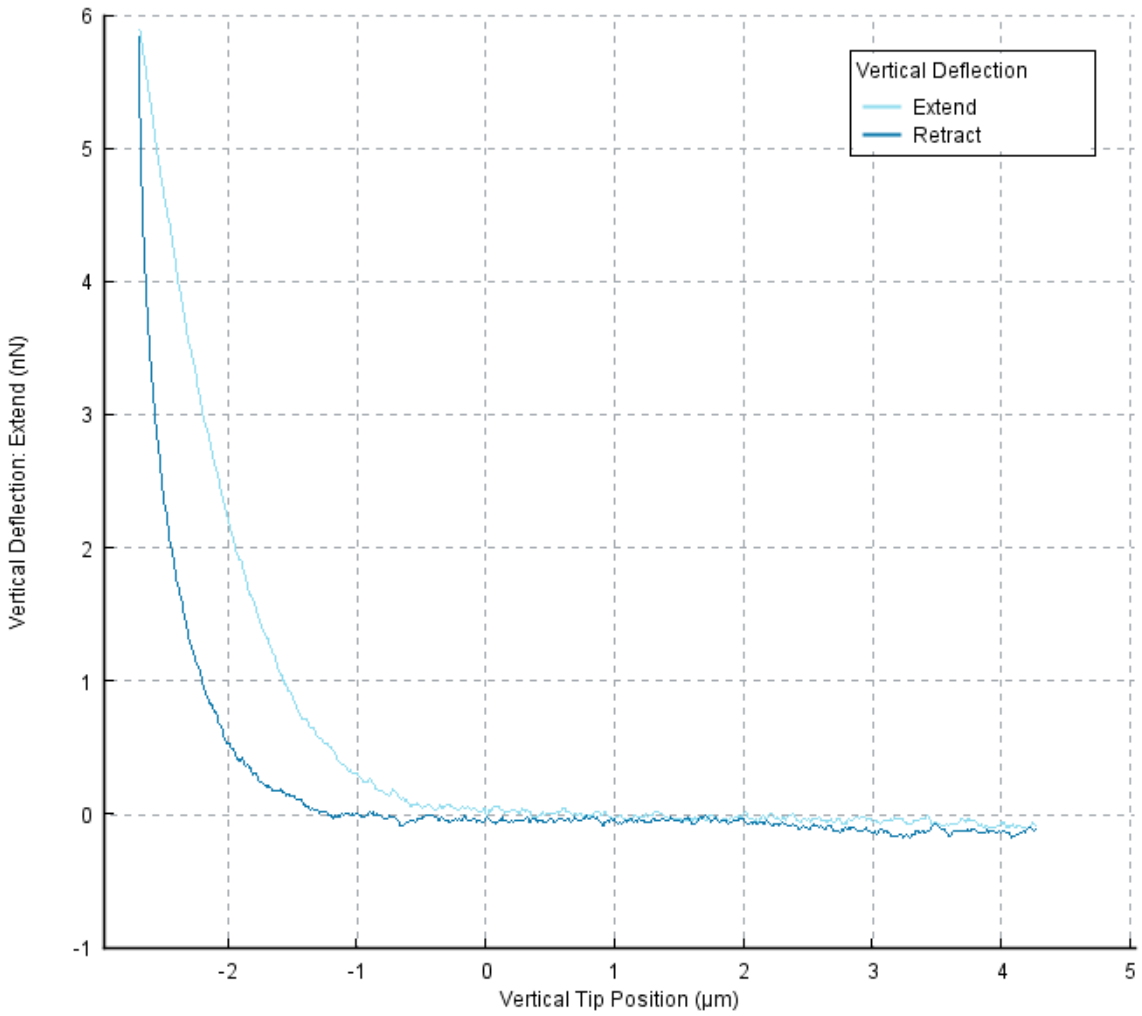

Figure A.5: Calculate the Tip-Sample Separation

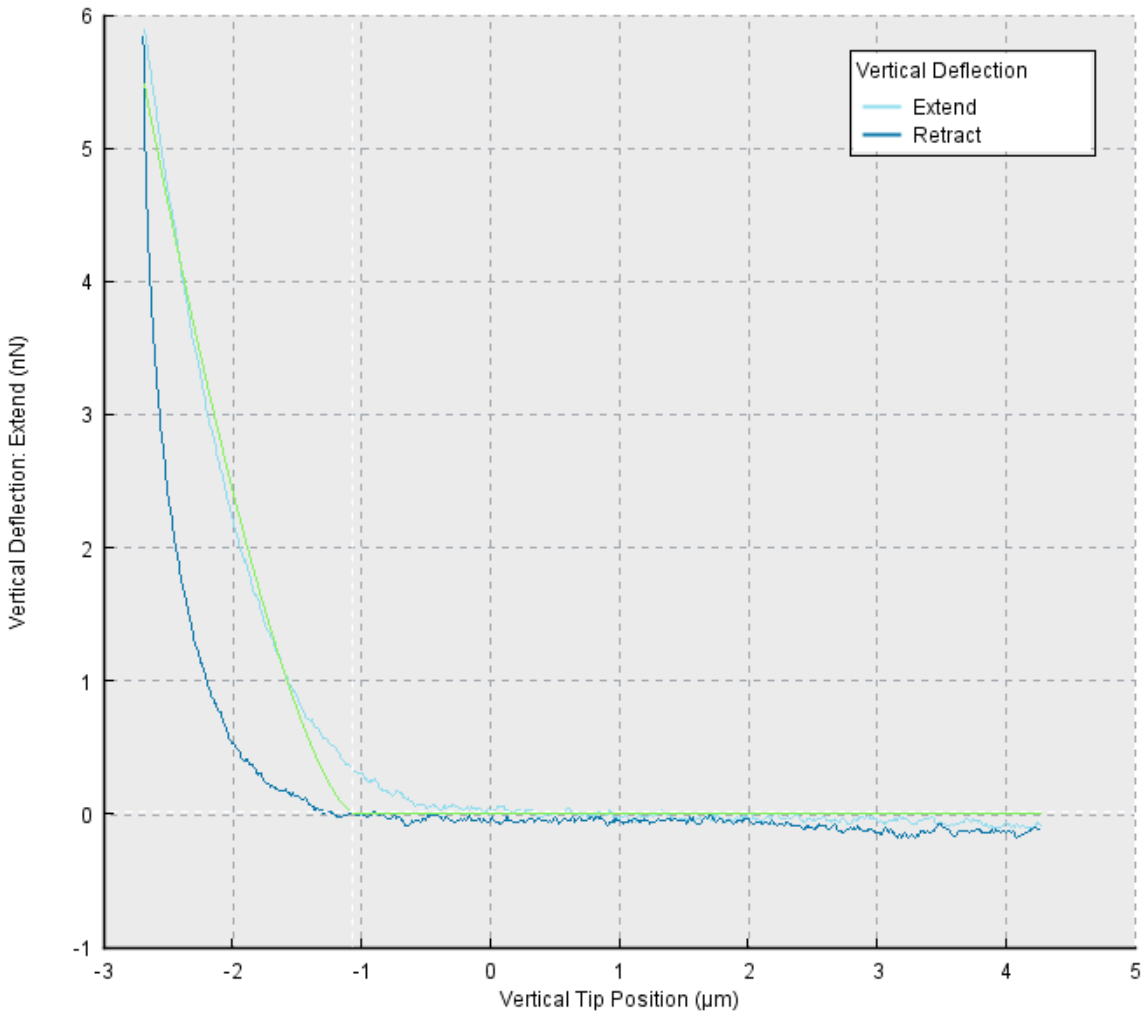

Figure A.6: Apply the Hertz Model to fit the Young's Modulus

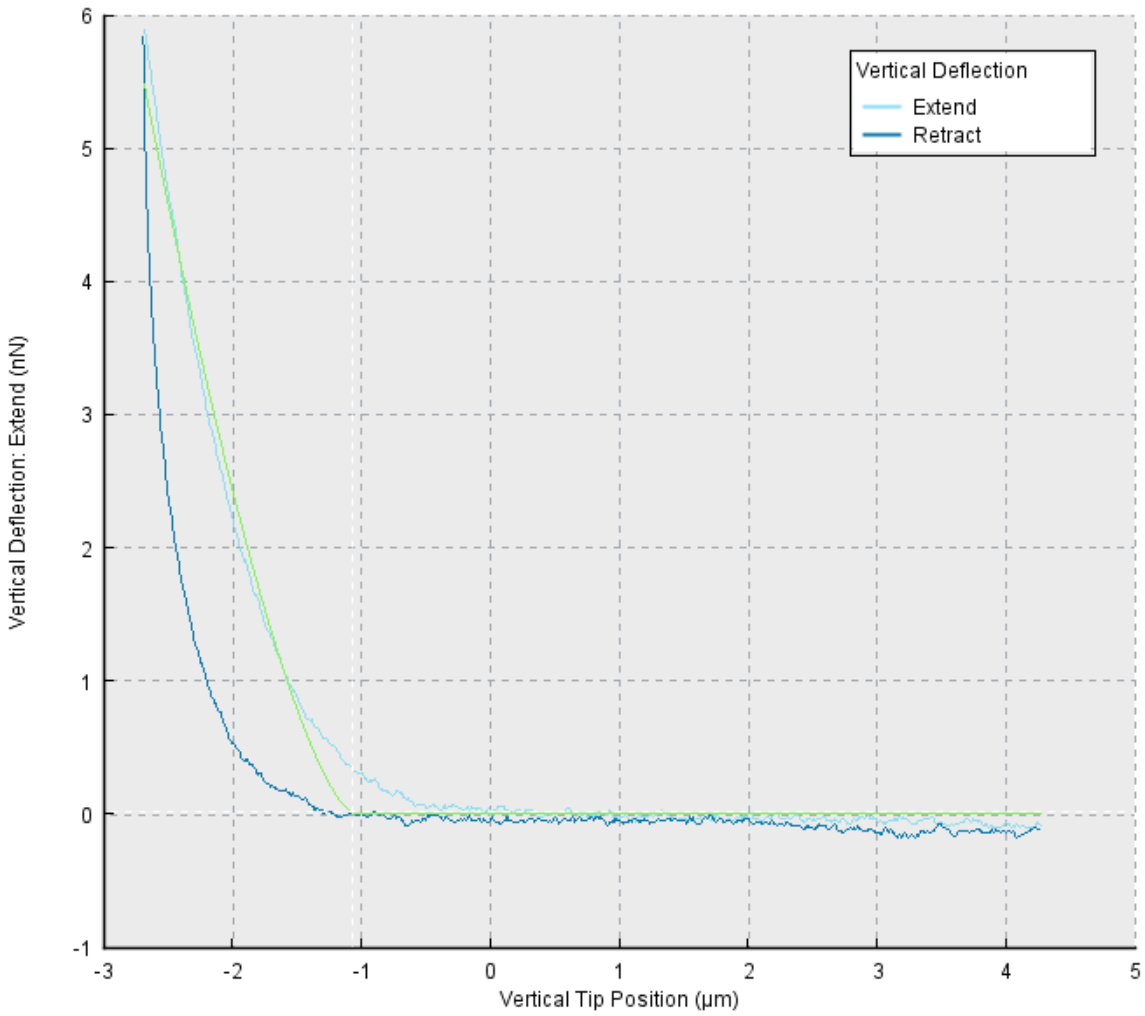

Figure A.7: Apply fitting range of 1 µm

B

Hydrogel force curve analysis

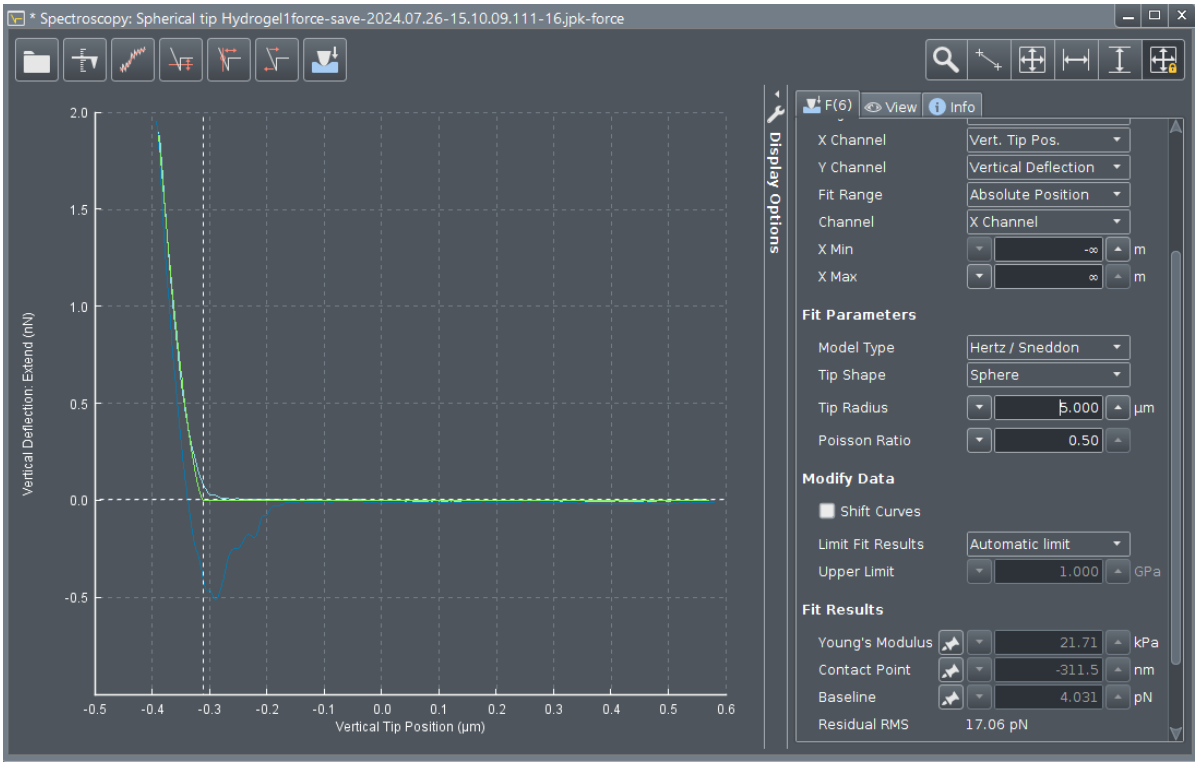

Figure B.1: Force curve on hyrdrogel with the fitted Hertz Model to obtain the Young' Modulus